Landau Damping Induced Limits in Nanogap Metal-Insulator-Metal Plasmonic Waveguides and Cavities

Thesis by

Daniel Rimoli Assumpcao

In Partial Fulfillment of the Requirements for

the degree of

BACHELOR OF SCIENCE IN

ELECTRICAL ENGINEERING

CALIFORNIA INSTITUTE OF TECHNOLOGY

Pasadena, California

2019

Daniel Rimoli Assumpcao

ORCID: 0000-0002-0374-9901

ACKNOWLEDGEMENTS

I would like to thank my thesis advisor, Dr. Hyuck Choo, for serving as my research advisor over the past four years. Your support and guidance over the years has helped me develop technically and personally as a researcher.

I also would like to thank Dr. Shailabh Kumar and Dr. Radwan Siddique for being my postdoctoral mentors during my time in Choo lab. You guys have taught me countless skills and have given me the guidance needed to be a successful researcher.

Finally, I would like to thank the Caltech SURF Office, the Caltech-GIST collaboration fund, Samsung Advanced Institute of Technology, and the Kavli Nanoscience Institute for providing support and facilities to me over the years.

ABSTRACT

Plasmonic structures permit the focusing of light into volumes far below the diffraction limit. In particular Metal-Insulator-Metal (MIM) gap plasmonic structures can reach nanoscale energy confinement if the gap is sufficiently miniaturized. Under classical models, gap plasmonics can achieve indefinite confinement, down to the single atom level. However, these classical models fail to consider quantum effects that occur as the confinement approaches the single nanometer level. Recently, it has been demonstrated that Landau Damping, the absorption of highly confined plasmonic energy, is the dominant effect in highly confined MIM devices until the tunneling regime is reached. However, the effects of Landau Damping on MIM gap devices are poorly understood. In this work, we analyze the effects of Landau Damping on MIM gap devices, specifically MIM waveguides and cavities. It is found that in waveguides, Landau Damping does not limit the confinement but does limit the maximum propagation length achievable. Moreover, in cavity structures, Landau Damping causes the Quality Factor to drop significantly as the gap is further miniaturized. In terms of quantum optics applications, this causes the radiative spontaneous emission enhancement to actually decrease as the gap is miniaturized sufficiently and a saturation of the coupling-loss ratio limiting the achievement of strong coupling . These effects will limit the possibilities for high performance nanogap plasmonic devices.

TABLE OF CONTENTS

LIST OF ILLUSTRATIONS AND/OR TABLES

NOMENCLATURE

Plasmonics: The study of the interaction of metals with light, and more specifically the coupling of light to the electrons in the metal. The field both explains the optical properties of metals helps to enable novel devices.

Surface Plasmon Polariton (SPP): An electromagnetic mode that exists at the interface between metals and dielectrics due to the coupling of incident photons and electrons in the metal. Unlike the electromagnetic modes of dielectric materials whose confinement is limited by the diffraction limit, SPPs can achieve energy confinement far below the free space wavelength of light. The confinement in an individual SPP mode is dependent on the materials and the incident free space wavelength.

SPP Gap Mode: A special type of SPP mode formed when two metals are separated by a dielectric gap. The individual SPPs on both interfaces interfere, forming a joint gap mode. Due to the interference, the confinement of the energy is localized to the gap and thus is dependent on the size of the gap.

Metal-Insulator-Metal (MIM): Specific type of gap mode formed through having two metals separated by an inner dielectric layer. The inner dielectric layer is referred to as the gap. This arrangement allows the increase of confinement through miniaturizing the gap. Under classical models, the confinement can be increased arbitrarily through further miniaturizing the gap. The primary goal of this work is to look at the practical limits to this confinement due to the onset of Landau Damping

Local / Classical Model: Refers to the use of classical electromagnetic expressions to describe plasmonic structures. Landau Damping is not taken into account in this model.

Landau Damping: Refers to in general the absorption of high wavevector waves in a plasma. In the context of plasmonic, refers to the absorption of highly confined electromagnetic energy in SPP modes due to the high wavevector enabling electronic transitions that were previously forbidden due to a momentum mismatch.

Intrinsic Damping: The damping in a material due to the material properties and in absence of Landau Damping.

Landau Damping Induced Damping: The damping induced by the onset of Landau Damping at high energy confinements. This summed with the intrinsic damping gives the total damping under the Landau Damping model.

Optical Waveguide: Structure that guides electromagnetic waves, restricting the expansion of the mode and thus the loss. They are integral to routing electromagnetic energy in highly compact settings, such as in integrated optical interconnects in integrated circuits.

Waveguide Mode: A solution to the electromagnetic differential equation describing a waveguide. It describes the distribution of the electromagnetic fields that will propagate in the waveguide. In this work, the mode always refers to the fundamental mode of the waveguide, meaning the one with no variation parallel to the metal-gap interface.

Wavenumber: The propagation constant of a waveguiding mode. The real part corresponds with the spatial frequency and the imaginary part with the losses.

Mode Length: A figure of merit for the confinement in a waveguide. It can be interpreted as the average length which the energy is spread over in a waveguide. It is calculated through dividing the total energy transferred in the waveguide by the energy at the center point.

Propagation Length: The length in the propagation direction over which the energy in the waveguide drops to 1/e of its initial value.

Optical Cavity: An electromagnetic resonator which stores optical energy through the interference of multiple reflection forming standing waves. Through placing matter in the cavity, the interaction between light and matter can be altered which has important applications in future quantum technology. The strength of the light and matter interaction in the cavity can be calculated through the cavity's mode volume and quality factor.

Cavity Mode: A solution to the electromagnetic differential equations governing the behavior of the cavity. It represents a distribution of the electromagnetic field which oscillates in time but whose distribution remains constant.

Constant-Gap MIM Cavity: The MIM cavity structure considered in this work consisting of two rectangular cuboid metals sandwiching an inner dielectric layer. The gap between the metals is constant throughout the structure.

Mode Volume: Parameter of a cavity mode which describes the confinement of energy in the cavity. It represents the average volume which the energy of the cavity is spread over for a given mode.

Quality Factor: Parameter of a cavity mode which describes the energy loss in the system. It is proportional to the number of oscillation cycles that the cavity can undergo before all energy in the system is lost.

Purcell Factor: Figure of merit indicating the strength of the light-matter interaction for an emitter placed in the cavity. It corresponds with the increase in the spontaneous emission rate of an emitter placed in the cavity due to the Purcell effect.

Purcell Effect: The enhancement of an emitter's spontaneous emission rate through changing its optical environment. In the context of this work, the rate is changed through putting the emitter in an MIM optical cavity.

Single Photon Source: Device which deterministically emits a single photon on demand. It is a crucial building block for quantum telecommunication technology.

Radiative Spontaneous Emission Enhancement: The increase in the Spontaneous Emission of an emitter radiated from the cavity. It differs from the Purcell Factor because it refers to only the increase in photons radiated from the cavity, ignoring photons absorbed by the cavity. It is important for creating bright single-photon sources.

Strong Coupling: Regime in which the emitter and its cavity are significantly coupled such that their modes are perturbed, forming hybrid modes. Qualitatively, this occurs when a photon emitted by the emitter in the cavity is more likely to be reabsorbed by the emitter than emitted from the cavity. Strongly coupled cavity-emitter systems have important applications in quantum information processing as well as creating novel light-matter devices.

Coupling-Loss Ratio: Parameter quantifying the ratio between the coupling rate between a cavity and emitter, and the total loss in the system. Increasing this parameter sufficiently allows the system to enter the strong coupling regime.

ABBREVIATIONS

MIM – Metal Insulator Metal

t – Gap thickness in MIM structure

L_{prop}- Propagation length of a waveguide mode

M – Mode length of a waveguide mode

L – Length of the cavity

Q – Quality factor of a mode of a cavity

V – Mode Volume of a mode of the cavity

F – Purcell factor of a mode of the cavity

rSE – Radiative Spontaneous Emission Enhancement

Chapter 1

INTRODUCTION TO PLASMONICS AND LANDAU DAMPING

Using fabricated nanostructures to control light on the nanoscale has opened entirely new possibilities in a variety of fields including on-chip electro-optic integration and optical interconnects for computation [1-3], single molecule biosensing for integrated medical implant technology [4-7], and empowering future quantum information technology [8-10]. This combination of nanotechnology with photonics, called nanophotonics, utilizes the ability to confine light to the nanoscale to achieve these exotic phenomena. The achievable confinement with traditional dielectric nanophotonic technology, however, is limited to the micron or hundreds of nanometer scale due to the diffraction of electromagnetic waves. Nevertheless, this limitation can be overcome with plasmonic structures.

Plasmonics, a cornerstone of nanophotonics, combine metals with traditional dielectrics to bypass the diffraction limit [11]. Specifically, a novel surface electromagnetic mode called a Surface Plasmon Polariton (SPP) is created at the interface of the metal and dielectric due to the coupling of photons and collective oscillation of electrons in the metal [11]. This mode is localized to the interface, permitting confinement far below the dielectric diffraction limit at the expense of large losses due to the optical ohmic losses in metals.

Individual SPP modes have confinements dependent on a variety of design parameters such as the metal and dielectric used, and the freespace wavelength. However,

by combining two SPPs in proximity in a gap configuration, the two modes will interfere allowing much smaller confinements to be achieved [11]. In particular Metal-Insulator-Metal (MIM) structures, consisting of two metals separated by an inner dielectric layer, can achieve extremely high energy confinements with a large portion of the energy localized to the insulator layer [12, 13]. Moreover, the confinement is geometrically dependent on the insulator gap size, allowing the gap to be shrunk for further confinement.

Due to the confinement achievable with plasmonics, a variety of novel applications have been developed including devices for confined on-chip computation [14-16], single molecule sensing with Surface Enhanced Raman Scattering (SERS) [17-19], planar optical metasurfaces [20-22], and single-photon sources [23-25] to name a few. In particular, integrated MIM waveguides and utilizing MIM cavities to increase light-matter coupling for quantum information applications have a large potential. They will now be discussed in detail to provide context for our work.

Applications of MIM Waveguides:

Electromagnetic waveguides guide the transmission of light from one point to another in a confined area. These devices have many uses, but one particularly impactful one is their integration into on-chip communications technology. Recently, dielectric waveguides have been integrated into electrical chips to provide intrachip and chip to chip communication at potentially faster rates while utilizing less energy than electrical interconnects [26]. However, when using dielectric materials, the size of the waveguide is limited by the diffraction limit. This limit, on the order of hundreds of nanometers, is far larger than the tens of nanometer size of modern-day transistors. There is a clear size

mismatch between the two that limits both the maximum density of optical interconnect technology and the ability to replace electrical interconnects. However, this limit can be overcome using plasmonic technology. The MIM mode can be used to construct waveguides unaffected by the diffraction limit. These MIM waveguides can be miniaturized far below the diffraction limit, and thus can be used to make compact on chip waveguides to potentially replace nanoscale electrical interconnects.

Beyond applications in on chip interconnects, the high confinement achievable with MIM waveguides permit new possibilities previously unreachable with dielectric material. For example, the confinement allows MIM waveguides to focus light and probe individual molecules. Already MIM waveguide structures have been integrated into scanning probes to permit single molecule spectroscopy [27, 28] and these devices can potentially be fabricated on chip to enhance single molecule detection for medical technology [14].

Applications of MIM Cavities for Quantum Plasmonics

Efficiently coupling of photons and atomic quantum emitter is a cornerstone for the realization of quantum information technology [24, 29]. Due to the comparatively small size of an atom as compared to the wavelength of light, the interaction between light and atomic emitters is normally weak. However, by integrating these emitters into electromagnetic cavities, which store electromagnetic energy within their confined volume, the light-matter interaction can be increased, and unique behavior can be attained. MIM cavities, formed by the truncation of an MIM waveguide, allow the confinement of energy far below that of dielectric cavities. Thus they can achieve large

cavity-emitter couplings [29]. Due to this, researchers have begun investigating these MIM cavities for quantum applications, forming the field of quantum plasmonics.

Two different regimes emerge depending on the strength of the cavity-emitter coupling. The first is the weak coupling regime. In this regime the spontaneous emission rate of the quantum emitter is increased through the Purcell Effect where the magnitude of the enhancement is dependent on the confinement of the cavity and its losses [29, 30]. This is particularly interesting for the creation of ultrabright single photon sources. Single photon sources, which deterministically emit a single photon a time, are a key building block of future quantum telecommunications technology [8]. However, the emission rate of quantum emitters, which act as single photon sources, is far too low to achieve practical communications technology. By coupling it to a cavity, this rate can be increased through the Purcell Effect. Plasmonic cavities are well suited for this, as theoretical work has shown they can achieve a two order of magnitude improvement over dielectric cavities due to their confinement [31]. Already there have been impressive experimental demonstrations of large rate enhancements, although larger enhancements are still desired [23, 25]. This is currently one of the primary objectives in quantum plasmonics [32].

If the cavity-emitter coupling is increased sufficiently, then the strong coupling regime is entered. In this regime, the coupling is sufficiently large such that the modes of the cavity and the emitter combine, permitting the control of matter using light for quantum information applications [33]. It has been difficult to achieve strong coupling with plasmonic nanocavities due to the large losses offsetting the high confinement [29]. Despite this, there has recently been demonstrations of single molecule strong coupling

at room temperature using an MIM cavity platform [34-37]. This platform can be further developed for both room-temperature quantum information applications as well as empowering novel light-matter interaction-based devices.

Quantum Mechanical Effects in Extreme Confinement Plasmonics

As seen above, there is a plethora of opportunities for MIM plasmonic devices all of which are enhanced by the extreme confinement achievable with the platform. Moreover, the performance of these devices is linked to the achievable confinement. However, the limits of confinement in these structures are poorly understood. Under the classical model, the energy of an MIM structure can be confined indefinitely through further miniaturization of the gap, allowing energy to be confined to atomic and subatomic volumes. However, this model fails to consider quantum mechanical effects that occur once the confinement approaches the nanometer level that may potentially limit performance [38]. These effects will be briefly reviewed here.

There are two effects that occur in highly confined nanogap MIM structures, plasmonic tunneling and Landau Damping. Tunneling occurs when the gap is sufficiently small so that charge can tunnel from one metal to another, creating another loss pathway that effectively eliminates the gap mode [39]. A combination of theoretical modeling and experimental work has demonstrated that tunneling begins to occur at optical frequencies in gaps of around 0.5nm [39-42]. Thus, it only occurs at extreme, potentially subatomic levels of confinement. Since a monolayer of many of the interatomic spacers that could be used for the fabrication of MIM structures is larger than this, tunneling is not necessarily technologically limiting.

At intermediate gap sizes between 0.5nm to around 10nm, Landau Damping occurs. In plasmonic dimers, researchers observed a shift and broadening of the resonances as compared to the classical models when gaps were in the above range. These were phenomenologically modeled as nonlocal effects. A variety of nonlocal phenomenologically models with increasing levels of sophistication have been proposed and matched to experimental results [43-45]. More recently, it was proposed that all these nonlocal effects can be attributed to Landau Damping [46]. In a plasmonic context, Landau Damping refers to the absorption of high wavevectors of plasmonic energy. When the spatial confinement of energy in a plasmonic structure is sufficiently high, the momentum of the SPP is large enough to drive previously momentum forbidden electronic transitions. This opens a new absorption pathway. Previous theoretical work demonstrated that the anomalous shift in nanosphere dimer systems could be explained by Landau Damping [47]. These effects occur at comparatively much larger gap sizes than tunneling, thus making it more significant to practical MIM technology. However, the effects of Landau Damping and the limits on performance it induces are poorly understood in many MIM systems.

Our Work

From the above discussion, MIM devices have very useful applications due to their confinement. Despite this, the limits on the performance of many fundamental MIM gap devices due to the introduction of quantum effects is poorly understood.

In this work, analytical and numerical techniques are used to study the effects of Landau Damping in MIM waveguides and constant-gap MIM cavities with single-

nanometer gaps. Moreover, we study how the magnitude of these effects can be changed through tuning of the wavelength and the dielectric constant of the inner dielectric. Finally, Landau Damping's impact on the suitability of waveguides and cavities for different applications is considered.

We determine that Landau Damping can be extremely harmful to the performance of nanogap plasmonic devices, limiting potential applications. Specifically, it is discovered that in MIM waveguides, Landau Damping does not limit the confinement but it both decreases and limits the maximum propagation length due to the introduction of the addition loss mechanism. In MIM cavities, this manifests as a significant drop in the quality factor as the gap is decreased. This causes the radiated Spontaneous Emission enhancement to decrease as the gap is miniaturized and the coupling-loss ratio for strong coupling to stagnate. In both platforms, it was found that using larger wavelengths and lower dielectric constants for the inner dielectric spacer minimized the effects of Landau Damping. This will be vital for the design and applications of future integrated plasmonic waveguides and nanocavities.

The thesis is organized as follows:

Chapter 2: The background of Landau Damping and studying the performance of MIM waveguides is discussed.

Chapter 3: An analysis of the effects of Landau Damping on MIM waveguides is presented

Chapter 4; The background for using Landau Damping to analyze MIM cavities is discussed.

Chapter 5: The effects of Landau Damping on MIM cavities is discussed

Chapter 6: Conclusion

Chapter 2

CALCULATING LANDAU DAMPING IN MIM WAVEGUIDES

Introduction

In this work analytical and numerical FEM simulations are used to determine the effects of Landau Damping in MIM plasmonic devices. Both are utilized since the analytical analysis provides an understanding of the reasoning behind the observed effects, but simulations allow for more robust results. This section discusses the background and methodology for integrating Landau Damping into traditional electromagnetic models for both the analytical and numerical calculations of the properties of MIM waveguides.

The device structure considered is shown in Fig 2a. It consists of an MIM waveguide with two metals sandwiching an inner dielectric layer of thickness *t*, and infinite in both the propagation direction and parallel direction. Beyond allowing us to study MIM waveguides, the behavior of MIM cavities is also calculated from the parameters of this model MIM waveguides as opposed to a direct calculation (see Chapter 4).

The relative permittivity of the metal was described by the Drude model [11]:

$$\varepsilon(\omega) = 1 - \frac{\omega_p^2}{\omega^2 + i\gamma_{intr}\omega} \qquad (2-1)$$

where ω is the incident frequency, and ω_p and γ are material properties referring to the plasma frequency and damping of the metal respectively.

Two metals were considered, Ag, whose parameters were taken from the literature [48], and an ideal metal where the intrinsic damping was set to 0. The gap, incident freespace wavelength, and permittivity of the inner dielectric were all varied. Only the fundamental mode of the waveguide is considered in this work.

There are three main parameters for a waveguide to understand its performance. First there is the wavenumber, *k* of the waveguide which is the propagation constant of the mode and gives a sense of the confinement in the propagation direction. Second there is the propagation length L_{prop}, which is defined as the length over which the plasmonic mode losses 1/e of its energy and corresponds with the loss of the waveguide. Finally, there is the mode length, *M*, of the mode which is the average length in the transverse direction which the energy is distributed over. It provides the best estimation of the transverse confinement of the waveguide. The exact expressions for these parameters are discussed below.

Classical Local Simulations

To solve for the waveguiding modes, a quasi 1D cross section of the waveguide was taken and the mode was solved for either using analytical or FEM simulations (COMSOL) [49]. Since a quasi 1D cross section was used, only the fundamental mode of the waveguide was solved for and all the calculations are based on the fundamental model. Fig 2b shows an example of a calculated electric field cross-section for an MIM waveguide

The simulation software solves the complex wavenumber k_{mode} of the waveguiding mode in addition to the E-field distribution. Then the different parameters of the mode can be calculated. The propagation length is given by [11]:

$$L_{prop} = (2Im[k_{mode}])^{-1} \quad (2-2)$$

The mode length is calculated from the distribution of fields of the mode along the 1D cross-section using the following equation [11].

$$M = \frac{\int u_e(x)dz}{u_e(x_0)} \quad (2-3)$$

where $u_e(x)$ is the energy density of the electric field at a position *x* and x_0 is the center of the waveguide. The energy density of the electric field at a position x for a Drude model metal is given by [50]:

$$u_e(x) = \frac{\varepsilon_0}{2}\left(n^2 + \frac{2\omega n\kappa}{\gamma}\right)|\boldsymbol{E}(x)|^2 \quad (2-4)$$

where $\boldsymbol{E}(x)$ is the electric field at a position x, and n, κ are the real and imaginary parts respectively of the index of refraction of the material at a position x. Note that although the above equation applies for Drude-model metals, it also applies to lossless dielectrics where $\kappa = 0$. Thus, in the context of the simulations in this work, it can be applied to the entire MIM structure.

Note that in this work, "local" and "classical" both refer to this model.

Landau Damping Model

To account for Landau Damping, the local model needs to be extended. This can be done by adapting the dielectric constant of the metal from the Drude model to consider

the increased absorption pathways induced by Landau damping. Note that the following derivation in this section was adapted from ref [46] and is not unique to this work.

A more complete expression for the dielectric constant of a metal is given by the Lindhard model:

$$\varepsilon(\omega, k) = \varepsilon_b + \frac{3\omega_p^2}{k^2 v_F^2}\left(1 - \frac{\omega}{2kv_F} ln \frac{\omega + kv_F}{w - kv_F}\right) \qquad (2-5)$$

Let $q = \frac{k}{k_{LD}}$ where $k_{LD} = v_F/w$ and corresponds with the offset vector for Landau Damping. Now notice that as q > 1, the imaginary part of the dielectric constant begins to increase leading to losses in the material and is given by:

$$\varepsilon_i(\omega, q) = \frac{3}{2}\pi \frac{\omega_p^2}{\omega^2 q^3} \qquad (2-6)$$

This increase in the losses of the material is due to Landau damping. Thus, we have an expression for the imaginary part of the dielectric constant due to Landau damping at a given wavevector. Given a distribution of the electric field, **E(**r**),** the longitudinal Fourier transform can be taken to determine the power density for a given wavevector using the following equation:

$$\left|F_{||}(k)\right|^2 = \frac{|\boldsymbol{F}(k) \cdot k|^2}{k^2} \qquad (2-7)$$

Where $\boldsymbol{F}(k)$is the Fourier transform of **E(**r**)**. Then, by computing the overlap of this power density with the expression for the induced losses at a given k, the total imaginary part ε_i induced by Landau Damping of can be expressed as:

$$\varepsilon_i = \frac{3\pi\omega_p^2}{2\omega^2} \int_1^\infty \frac{q^{-3}\left|F_{||}(q)\right|^2 dq}{\int_0^\infty |\boldsymbol{F}(q)|^2 dq} \qquad (2-8)$$

This loss can be incorporated into the Drude model through adding an additional damping term γ_{LD} so that the modified Drude model is given by:

$$\varepsilon(\omega) = 1 - \frac{\omega_p^2}{\omega^2 + i(\gamma_{intr} + \gamma_{LD})\omega} \qquad (2-9)$$

Since in the Drude model, $\varepsilon_i = \frac{\omega_p^2}{\omega^3}\,\gamma_{LD}$, γ_{LD} can be related to the **E(r)** and computed through the following formula:

$$\gamma_{LD} = \frac{3\pi\omega}{2}\int_1^{\infty} \frac{q^{-3}\left|F_{||}(q)\right|^2 dq}{\int_0^{\infty}|\boldsymbol{F}(q)|^2 dq} \qquad (2-10)$$

The above analysis demonstrates two points. First, the effects of Landau Damping can be fully accounted for using classical electromagnetic calculations based on the Drude model through adding an additional damping term to the models. Second, the additional damping term can be calculated from the electric field distribution of a mode using the formulas given above. This provides both the initial expressions from which the analytical expressions can be derived and a numerical method that can be implemented using FEM simulations.

Landau Damping Simulation Methodology

To implement the above formulas into FEM software, an iterative approach was used in ref [47] (Fig 2c). Initially the modes of the waveguide were calculated using just the intrinsic damping and not considering the Landau Damping induced damping rate. After this, the field profile of this mode was taken and from it the Landau Damping

induced damping rate, γ_{LD}, was calculated using (2-10). This Landau Damping induced damping rate was then combined with the intrinsic damping to calculate the new permittivity of the metals, and the simulation was repeated. This whole cycle was repeated until the value for γ_{LD} converged.

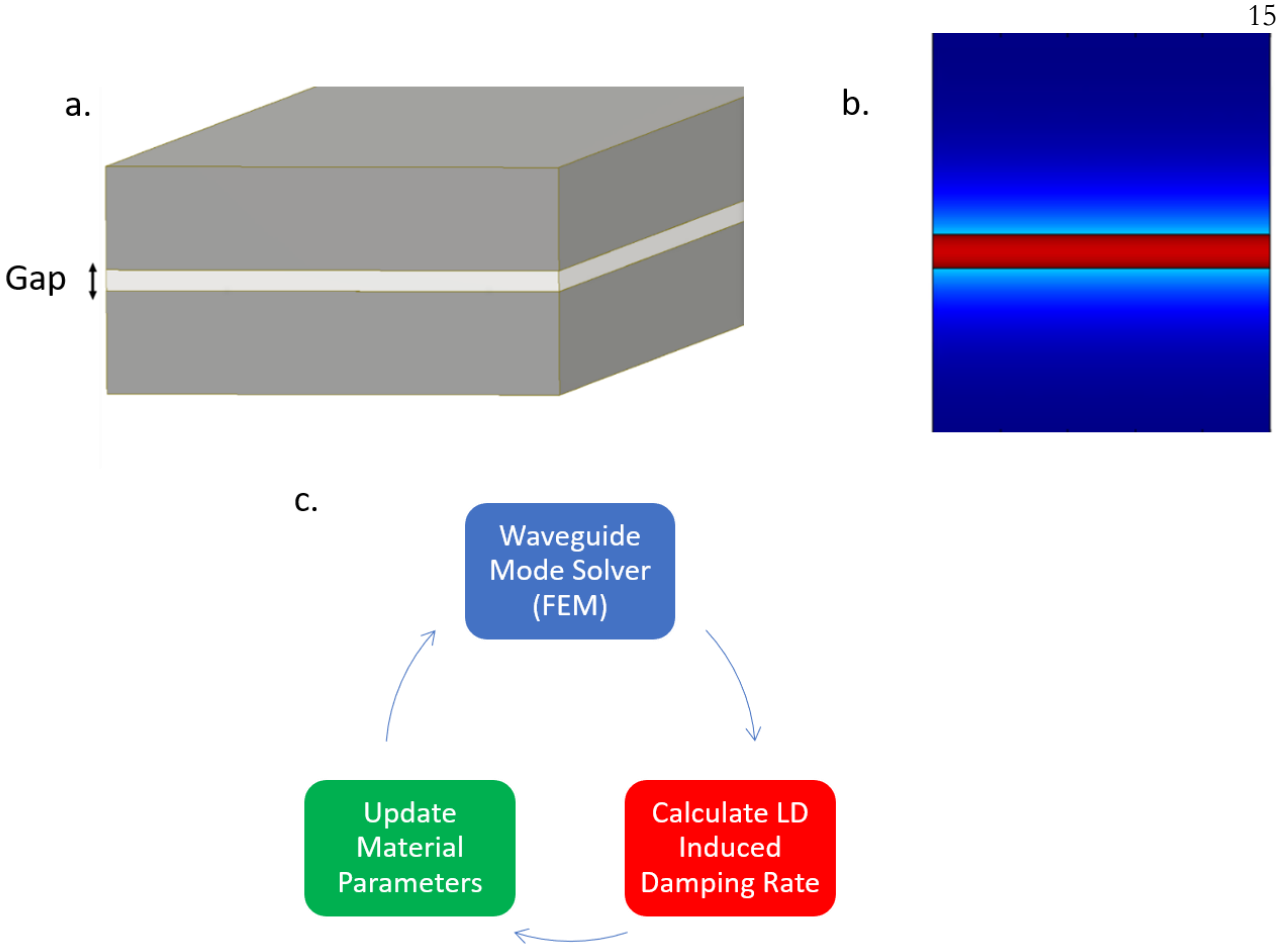

Figure 1: Diagram of Methodology. a. Diagram of the model Metal-Insulator-Metal waveguide considered in this work consisting of two metals sandwiching an inner dielectric layer with variable gap thickness. Note that the waveguide is infinite in all directions but the transverse (gap) direction. b. A plot of the electric field intensity distribution for an example fundamental mode of the MIM waveguide, showing most of the electric field is concentrated in the dielectric gap with no variations parallel to the metal-air interface. c. The methodology for simulating the behavior of the waveguide when considering the Landau Damping induced losses. An iterative approach is used, where the waveguide mode is first solved under the local model, the induced Landau

damping rate due to the E-field distribution is calculated, and then this additional damping term is incorporated back into the metal's optical parameters and the simulation is repeated. This is repeated until the damping term converges.

Chapter 3

EFFECTS OF LANDAU DAMPING IN MIM WAVEGUIDES

The MIM waveguide is the most fundamental gap plasmonic device. It has important applications and can be used to describe more sophisticated MIM plasmonic devices [15, 51]. The high confinement is key to the performance of these waveguides, and thus it is important to understand both how Landau Damping introduced at these high confinements limits the performance and how the waveguides can be engineered to overcome these limitations.

Analytic Description of Damping in MIM Waveguides

First we derive an analytical expression for the damping rate induced by Landau Damping in MIM waveguides at high confinements Since Landau damping does not change the wavenumber of the waveguiding mode (see simulations below), the relation between the wavenumber of the mode and the induced damping rate can be combined with the dispersion relation of MIM waveguides to provide an accurate analytical solution. This allows a more concrete understanding of the trends of Landau damping in waveguides than could be provided by simulation results alone.

It will be assumed that $k_{mode} \ll k_{LD}$ where k_{LD} is the offset vector for Landau Damping as given by $k_{LD} = v_F/w$. This assumption is valid because k_{LD} corresponds with spatial frequencies of ~0.5nm, which is well below most waveguides considered in this work.

The magnitude of the electric field perpendicular to the propagation direction within the metal can be written as [11]:

$$E_{perp} = Ck_{mode}e^{-k_{perp}x} \quad (3-1)$$

Where C is a proportionality constant, k_{perp} is the decay rate of the field in the metal, and x is the position in the metal where 0 is defined at the metal-dielectric interface.

Similarly, the electric field in the direction of propagation is given by [11]:

$$E_{parallel} = -iCk_{perp}e^{-k_{perp}x} \quad (3-2)$$

The perpendicular wave vector can be related to the wavenumber of the mode through the wave equation [11]:

$${k_{perp}}^2 = k_{mode}^2 - \left(\frac{2\pi}{\lambda}\right)^2 \varepsilon_m \quad (3-3)$$

If we assume high confinement, then $k_{mode} \gg \left(\frac{2\pi}{\lambda}\right)^2 \varepsilon_m$ so $k_{perp} \approx k_{mode}$ and thus $|E_{perp}| = |E_{parallel}|$, simplifying the calculation

Next the spatial power density for either the parallel or perpendicular direction is calculated by taking the Fourier transform of the electric field distribution:

$$F(k) = \frac{Ck_{mode}}{k_{mode} + ik} = \frac{C}{1 + i\frac{k}{k_{mode}}} \quad (3-4)$$

Where k is the spatial wavevector perpendicular to the metal-dielectric interface. The longitudinal Fourier transform is given by (2-7):

$$|F_{||}(k)|^2 = \frac{|\boldsymbol{F}(k)\cdot\boldsymbol{k}|^2}{k^2} = \frac{|F_{perp}(k)\cdot k|^2 + |F_{parallel}(k)\cdot k_{mode}|^2}{k^2} \quad (3-5)$$

However, note our earlier assumption that $k_{mode} \ll k_{LD}$. This ensures that when the integral of the longitudinal transform is taken, $k_{mode} \ll k$ and thus the parallel field contribution to the Landau Damping can be neglected to obtain:

$$\left|F_{||}(k)\right|^2 = \left|F_{perp}(k)\right|^2 \qquad (3-6)$$

The final step is to evaluate the two integrals in the equation for the Landau Damping induced damping (2-10). We assumed that $k'_{mode} \gg k''_{mode}$ to simplify the calculation. These integrals will be evaluated individually:

$$\frac{1}{k_{LD}}\int_0^\infty |\boldsymbol{F}(k)|^2 dk = \frac{1}{k_{LD}}\int_0^\infty \left(\left|F_{parallel}(k)\right|^2 + \left|F_{perp}(k)\right|^2\right) dk = \frac{C^2}{k_{LD}} \cdot \pi k'_{mode}$$

$$\frac{1}{k_{LD}}\int_{k_{LD}}^\infty \left(\frac{k}{k_{LD}}\right)^{-3} \left|F_{||}(k)\right|^2 dk = k_{LD}^2 \int_{k_{LD}}^\infty k^{-3} \frac{C^2}{1+\left(\frac{k}{k'_{mode}}\right)^2} dk$$

$$\approx k_{LD}^2 C^2 \int_{k_{LD}}^\infty k^{-3} \frac{1}{\left(\frac{k}{k'_{mode}}\right)^2} dk = k_{LD}^2 C^2 k_{mode}^2 \int_{k_{LD}}^\infty k^{-5} dk$$

$$= \frac{C^2 (k'_{mode})^2}{4k_{LD}^2} \qquad (3-7)$$

The simplification in the second integral is due to the earlier assumption that $k_{mode} \ll k_{LD}$. Finally, evaluating the induced damping:

$$\gamma_{LD} = \frac{3\pi\omega}{2}\int_1^\infty \frac{q^{-3}\left|F_{||}(q)\right|^2 dq}{\int_0^\infty |\boldsymbol{F}(q)|^2 dq} = \frac{3}{8} v_f k'_{mode} \qquad (3-8)$$

Thus at large confinements, the induced damping in MIM waveguides is proportional to the real part of the wavenumber of the mode. The wavevector for an MIM mode is given by [52]:

$$k_{mode} = \frac{2\pi}{\lambda}\sqrt{\varepsilon_g + 2\zeta\left[1 + \sqrt{1 + \frac{\varepsilon_g - \varepsilon_m}{\zeta}}\right.} \qquad (3-9)$$

Where ε_g is the dielectric permittivity of the gap, ε_m is the permittivity of the metal, and

$$\zeta = \left(\frac{2\pi\varepsilon_m}{\lambda\varepsilon_g}t\right)^{-2} \qquad (3-10)$$

Thus, by iteratively solving both equations, γ_{LD} can be numerically estimated. However, since additional damping does not significantly change the real wavenumber of an MIM mode, k_{mode} can be computed using the intrinsic damping constants and then used to calculate γ_{LD} without significantly sacrificing accuracy, permitting the above to give an accurate analytical solution.

Performance of MIM Waveguides with Decreasing Gap Sizes

Having now an expression for the induced damping, FEM simulations under the classical and LD models (see section 2), were performed to numerically verify the analytical expression and understand its ramifications. The fundamental mode of an infinite Ag-air-Ag waveguide at an incident free space wavelength of 850nm was considered while the thickness of the gap, *t*, was varied.

Both the simulated induced damping rate due to Landau damping as well as the value calculated using the analytical equations are displayed in Fig 1a. The analytical expression shows excellent agreement with the FEM simulations, particularly at small gaps where the high confinement assumption is most valid.

We observe that the surface damping increases as the gap is miniaturized, due to the increased energy confinement. At a gap of 1nm, the LD induced damping rate has exceeded the intrinsic damping of Ag of ~$3\cdot10^{13}$, becoming the dominant loss mechanism.

Empirically, the Landau damping rate is roughly proportional to the inverse of the gap length. As an MIM waveguide is further miniaturized, the analytical expression for its wavenumber given by 3-9 approaches a simpler form [51]:

$$k_{mode} \approx -\frac{2\varepsilon_g}{\varepsilon_m t} \qquad (3-11)$$

Since the induced damping is proportional to the real part of the wavenumber, we observe that

$$\gamma_{LD} \approx Re\left(-\frac{3}{4}\frac{v_f \varepsilon_g}{\varepsilon_m t}\right) \approx -\frac{3}{4}\frac{v_f \varepsilon_g}{\varepsilon_m' t} \propto \frac{1}{t} \qquad (3-12)$$

Thus explaining the empirically observed $\propto \frac{1}{t}$ dependence of the damping rate at small gap sizes.

Having verified the accuracy of the analytical expression and FEM simulations, the simulations were used to understand the effects Landau Damping caused through computing the different properties of the waveguide mode. The dispersion relationship of the mode shows no change due to the inclusion of Landau Damping as opposed to the local model (Fig 1b). Mathematically, this is since the additional damping term primarily causes a change in the imaginary part of the dielectric constant. Thus, the real part of the mode, the wavevector, is left unchanged. Therefore the analytical expression for the Landau Damping model need not be solved iteratively to obtain to high accuracy.

The propagation length in the Landau Damping model, on the other hand, is considerably smaller than under the classical models particularly at small gaps (Fig 1c). At 1nm, the propagation length is half of what is predicted by the classical model. To understand the ramifications of this, an MIM waveguide with an ideal metal with no intrinsic loss was

considered. Under classical models this lossless waveguide would have an infinite propagation length, providing a solution for plasmonics' biggest issue. Under the Landau Damping model, however, loss is introduced due to Landau Damping and the propagation length is below a micron at a gap size of 1nm. The fact that an ideal, lossless model still has such a low propagation length due to Landau Damping indicates that Landau Damping caps the maximum achievable propagation length. Moreover, at small gap sizes, the maximum achievable performance is not significantly better than can what be currently achieved with Ag.

Finally, the effect Landau Damping has on energy confinement was considered through calculation of the mode length of the waveguide (Fig 1d). No change is seen between the mode length calculated for both the classical models and Landau Damping models. Thus, in these MIM waveguides, Landau Damping does not limit the maximum achievable confinement. This fact had previously been proposed in ref [47], where it was expressed that due to the boundary conditions of an MIM waveguide, the mode would be unable to spread out unlike what was seen in other systems. This also can be explained by the lack of change in the wavevector. At high confinements, (see Analytical sections), $k_{perp} \approx k_{mode}$ where k_{perp} is the rate of exponential decay of the electric field. A lack of change in the wavevector between the two models indicates no significant change in k_{perp}, corresponding with a lack of change in the achieved confinement. Thus, Landau Damping does not limit the confinement and the only limit to the confinement achievable with MIM waveguides is due to the onset of tunneling at ~0.5nm (see Appendix).

Performance of MIM Waveguides with Different Wavelengths

Beyond understanding how Landau Damping affects the performance of MIM waveguides, it is crucial to understand how the magnitude of these effects can be altered through playing with different parameters of the waveguide, specifically the incident wavelength and the inner dielectric used.

The magnitude of Landau Damping versus changes in the incident freespace wavelength was simulated where the gap was fixed to 1nm (Figure 2). We observe that the induced damping rate is increased as the wavelength is decreased and again showing good agreement between the FEM simulated damping rates and the analytical expressions (Figure 2a). In the expression for γ_{LD}, the only wavelength dependent term is k_{mode}. It was also observed that the wavenumber does increase with smaller wavelength (Figure 2b). Thus, the increase in k_{mode} as the wavelength increases leads to additional confinement within the metal and that is fully responsible for the higher damping.

The propagation length versus wavelength was calculated (Figure 2c). The propagation length is significantly longer for larger wavelengths due to the much smaller induced damping rate. For example, at a gap of 1nm and wavelength of 1550nm, the propagation length was 2 microns for the ideal case, four times the propagation length at a wavelength of 850nm. This provides one avenue for minimizing the impact of Landau Damping, as at longer wavelengths even at a gap of 1nm, the propagation length is still comparatively large.

The wavenumber and mode length were calculated, and no significant change is seen through the introduction of Landau Damping as before (Figure 2b/d). The mode length

shows a slight increase at smaller wavelengths as has been observed in the literature, but the magnitude of the change is comparatively small.

Performance of MIM waveguides with Varying Inner Dielectric Constant

The effect of the dielectric constant of the inner dielectric on the performance of MIM waveguides was examined. The value of the dielectric constant was varied with the gap fixed at 1nm and the wavelength fixed at 850nm (Figure 3).

The LD induced damping rate is shown in Figure 3a. An increase in the dielectric constant leads to a significantly larger damping rate. The increase in the dielectric constant leads to a larger wavevector of the mode which causes higher confinement of the electric field within the metal and thus a higher induced damping rate (Figure 2b). Looking at the analytical expressions, the wavevector of the waveguide mode at high confinements $k_{mode} \propto \varepsilon_g$ (3-11), and thus $\gamma_{LD} \propto \varepsilon_g$, explaining the quasi-linear relationship with the inner dielectric constant observed in both the wavenumber and induced damping rate. Note that at high values of the dielectric constant, the analytical induced damping term and the simulated damping diverge due to the extremely high wavenumber of the mode challenging the $k_{mode} \ll k_{LD}$ assumption made in the analytic derivation.

The magnitude of this change in the damping rate is quite large as the inner dielectric increases due to this linear relationship. For example, at a gap of 1nm, the induced damping rate is an order of magnitude higher for an inner dielectric constant of 12 then it is for an 1nm gap with an inner dielectric constant of 1. These dielectric constants roughly corresponds to the constants of a high-index semiconductor such as GaAs and air, respectively.

We examined the effect of this increased Landau Damping on the propagation length (Figure 3b). The increased Landau Damping at larger dielectric constants leads to a significant drop in the propagation length. At a gap of 1nm and an inner dielectric constant of 16, the propagation length is around 2nm, a tiny amount over an order of magnitude lower than what the classical model predicts and two orders of magnitude lower than what is achieved at a dielectric constant of 1. This demonstrates how detrimental Landau Damping can be to the operation of waveguides, particularly high index waveguides.

Discussion

From the above results, Landau Damping's biggest effect is that it severely limits the maximum achievable propagation length. Moreover, for small gap sizes this maximum propagation length is not much better than what can be achieved using low loss bulk metals such as Ag, indicating no potential significant improvement from a materials perspective

This point is particularly impactful for using MIM waveguides in integrated photonic applications to compactly send information at high densities. For intrachip and inter-chip communication, the information must be sent over a non-negligible distance larger than the 1 micron achievable at a gap of 1nm. This provides a practical cap on the minimum usable gap size that is dependent on the minimum propagation length required.

However, the results also demonstrate that through choose the design wavelength as well as inner dielectric intelligently, the effects of Landau Damping can be minimized, maximizing the optimal propagation length. For example, the simulations assumed a wavelength in the 850nm fiber optic band, but if larger wavelengths are used such as the C-

band (1550nm) the optimal propagation length can be increased by almost an order of magnitude (see Appendix for additional simulations at 1550nm). Moreover, the inner dielectric should be kept as low as possible to minimize the induced damping rate. Through engineering of these properties, plasmonic MIM waveguides can find a use for compact, short distance information transfer and then potentially integrated with dielectric waveguides for longer distance information transfer. Finally, 2D materials do not display this same out of plane Landau Damping and thus could be investigated as a possible avenue for overcoming this limit [53].

The onset of Landau Damping does not provide a limit on the achievable confinement, however. Thus, the gap can be miniaturized down to 0.5nm, at which the loss due to tunneling becomes dominantly lossy (see Appendix). This ensures bulk metal MIM waveguides can focus light down to the single atomic layer, the ultimate limits of confinement. Not only does this permit high-density integrated waveguides as discussed above, it also permits the focusing of light to probe individual molecules for sensing applications or fundamental study. Thus, the fundamental benefit of plasmonics, the extreme confinement achievable, is not limited by Landau Damping.

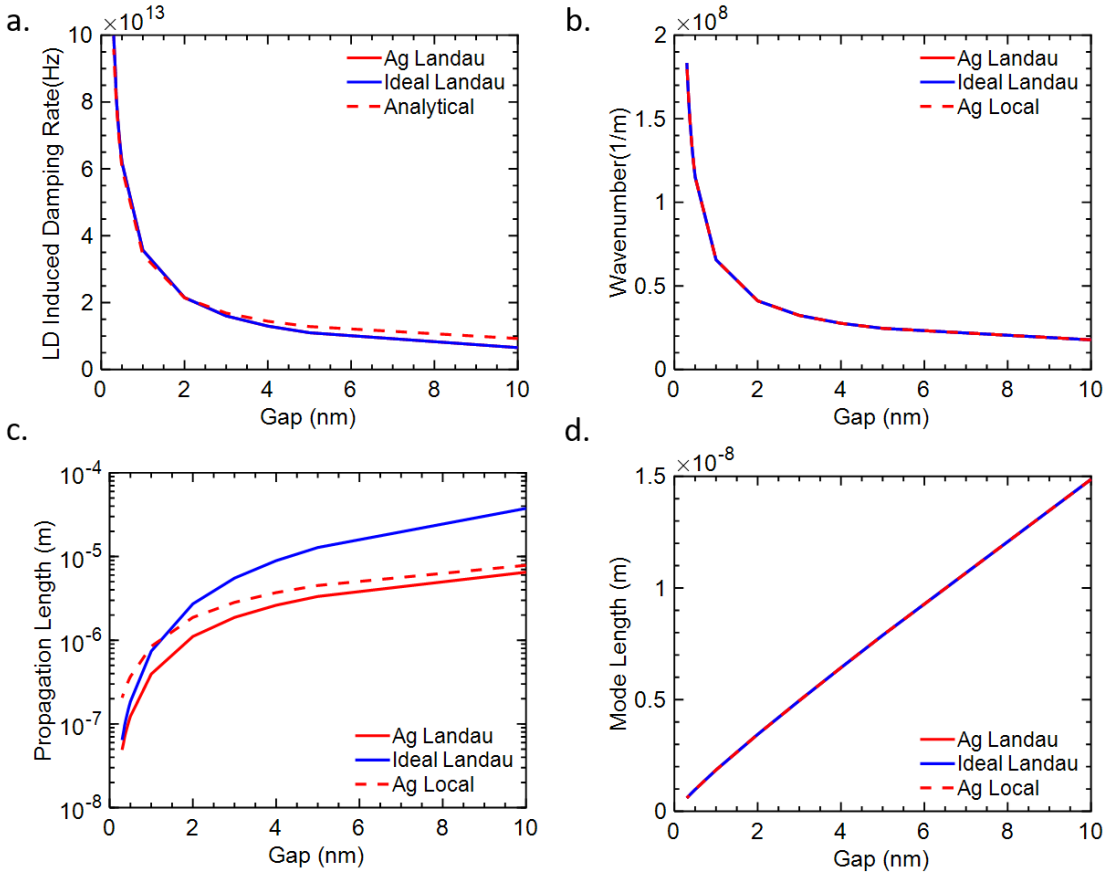

Figure 1. Properties of the MIM waveguide versus gap thickness. a. The induced Landau damping rate simulated for an Ag and an ideal metal waveguide as a function of gap thickness (curves are overlapped) as well as calculated using the analytic formula. The damping rate significantly increases as the gap is miniaturized and exceeds the intrinsic damping of Ag at 1nm. There is good agreement between the analytic and simulated values, particularly at small gap values. b. The wavenumber of the mode versus gap thickness for Ag under the classical local model and the Landau Damping model, showing no significant difference. c. Propagation length versus gap size for Ag under the classical and Landau Damping models, as well as an ideal metal with no intrinsic damping under the Landau damping model. Landau Damping causes a significant decrease in the propagation length of the waveguide, and

severely limits the maximum achievable propagation length as seen from the ideal metal's propagation length. (d) The mode length of the waveguide, showing no change between the Landau Damping and classical models. This indicates that Landau Damping does not limit the achievable confinement in the waveguide.

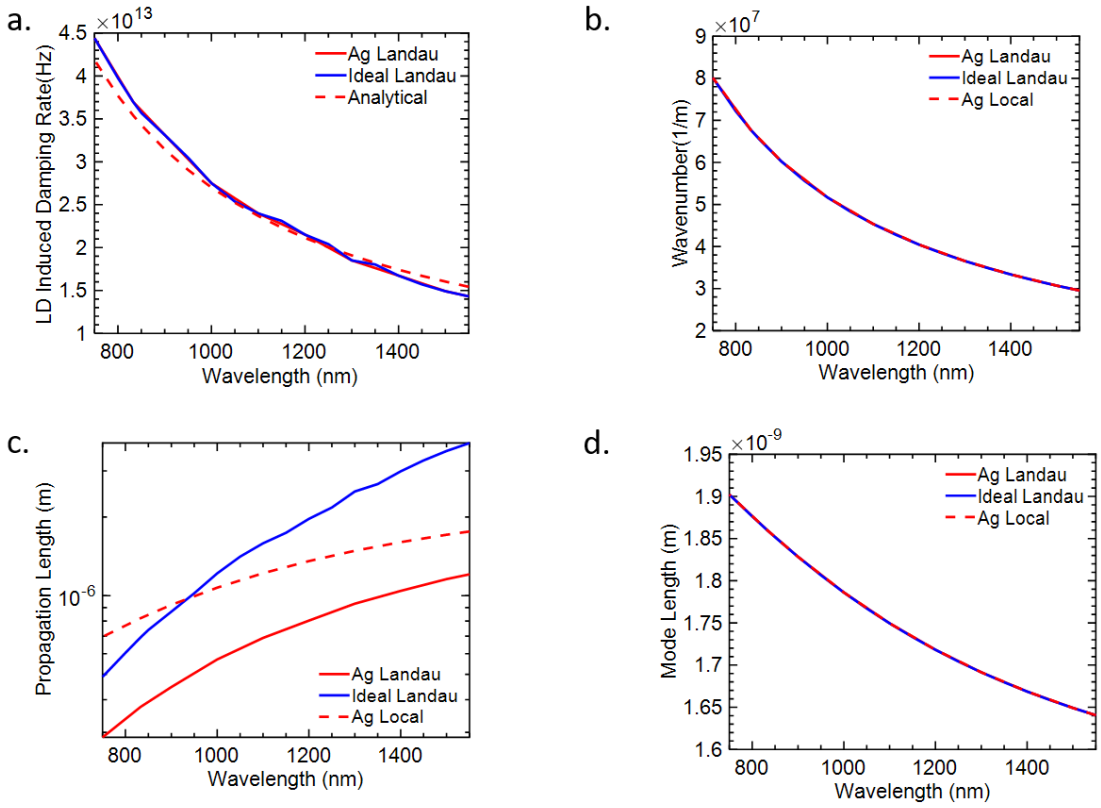

Figure 2: Properties of the MIM waveguide versus incident wavelength. a. The Landau Damping induced damping rate versus wavelength, showing an increased damping rate as the wavelength is shortened. b. Wavenumber versus wavelength, again showing no change between the classical and Landau Damping models and following the same trend at small wavelengths as seen in the induced damping rate. c. The propagation length versus wavelength, showing a considerable improvement at longer wavelengths due to lower induced Landau Damping rate. This provides one possible avenue to limit the effects of Landau Damping. d. The mode length versus wavelength, again showing no change between the classical and Landau Damping models and showing a comparatively small dependence on the wavelength.

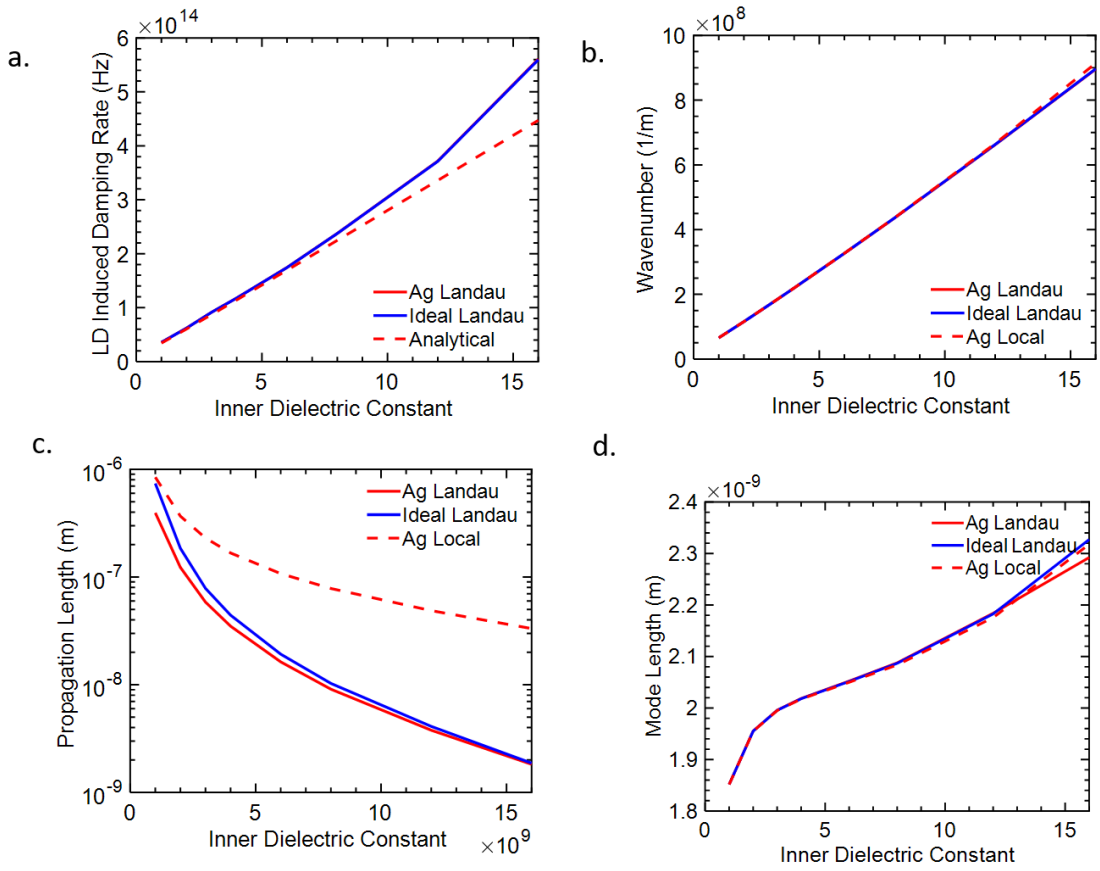

Figure 3: Properties of the MIM waveguide versus inner dielectric constant. a. The Landau Damping induced damping rate versus inner dielectric constant, showing a large, quasi-linear increase as the dielectric constant increases. The analytical and simulation values diverge at large dielectric constant values due to the violation of the assumptions the analytical solution was based on. b. Wavevector versus inner dielectric constant, showing a linear increase which explains the large increase in the induced damping rate. c. The propagation length versus inner dielectric constant, showing a significant decrease and a sub-10nm propagation length at high dielectric constants. d. The mode length of the simulated waveguides, showing only slight changes as the dielectric constant is varied.

Chapter 4

BACKGROUND ON METAL-INSULATOR-METAL CAVITIES

When a waveguide is truncated, the light is reflected at the truncated end, causing light to be trapped in the device and thus forming a cavity. This localizes the energy to the center of the structure, enhancing the interaction between light and matter and enabling many quantum optics applications [29]. Plasmonics, due to their high confinement, are particularly suitable for this application.

In this section, the background methodology for analyzing constant-gap MIM plasmonic cavities is discussed. The two key cavity parameters, the quality factor and mode volume will be calculated. Moreover, these cavities' suitability for two potential quantum optics applications: single photon sources and achieving strong coupling between light and matter, will be analyzed. Due to the large number of variables and assumptions in this section, analytical expressions will not be rigorously derived and instead will just be used to explain trends through proportionality arguments. In addition, the focus will be on trends as opposed to absolute values to ensure the generality of the results. This chapter goes over the methodology and the actual results are in the next chapter.

Rectangular cuboid constant-gap MIM cavities were considered (Fig 1). They consist of two finite length metals sandwiching an inner dielectric gap layer, which is just the waveguide considered previously but now truncated in the two infinite dimensions. The gap is constant across the cavity, allowing it to easily be described by the underlying waveguiding mode. The width was fixed to 350nm, a varying gap was used, and finally the length was set

such that the first order resonance in the length direction occurred at the chosen wavelength. This was done by setting the length to:

$$L = \frac{\pi}{Re\big(k(t)\big)} \qquad (4-1)$$

Where L is the length of the cavity, and k is the wavenumber of the MIM mode with gap size *t* . This is done so that the first resonance will still occur at the design wavelength regardless of the gap size or other parameters used. Thus, only the first resonance is ever considered in this work. In addition, it should be noted that the only modes of concern are those that are confined in the small gap layer which vary only along the length direction.

There are two primary parameters for cavities, the mode volume (V) and the quality factor (Q). V, similar to the mode length for waveguides, is the average volume which the energy is spread out over, quantifying the confinement. A smaller V indicates smaller confinement, and thus better coupling to emitters for quantum optics applications. Q quantifies the loss of the cavity, specifically referring to the ratio between the power stored in the resonator and the power lost per oscillation. A higher Q indicates the energy is stored in the cavity longer, allowing for better coupling to an embedded emitter and thus superior for quantum optics applications. A dimensionless figure of merit, the Purcell factor can be defined that is proportional to the Q/V of the cavity. The Purcell Factor refers to the proportion of spontaneous emission increase for an emitter placed within the cavity due to the Purcell Effect.

Q and V were calculated based on the mode parameters of their waveguiding cross section. This is done by considering the cavity as a traditional Fabry Perot cavity whose propagation characteristics are defined by the modes of the underlying waveguide. This allows us to apply the intuition built up in the previous chapter to this new domain.

The Q of the primary resonance of an MIM cavity can be related to its cross-sectional waveguiding parameters through the following equation [51]:

$$Q = \frac{2\pi n_g L}{\lambda\left(1 - \sqrt{R}e^{-\frac{L}{2L_p}}\right)} \qquad (4-2)$$

Where n_g is the group velocity and is given by $n_g = \frac{2\pi}{\lambda \cdot k(G)} - \lambda \frac{\partial}{\partial \lambda}(\frac{2\pi}{\lambda \cdot k(G)})$, λ is the free space wavelength, L_p is the propagation length, and *R* is the reflectivity at the air-MIM interface. The value of *R* was computed using FDTD simulations (see Appendix). The phase change of this reflection was assumed to be negligible. To evaluate the derivative for the group velocity, the analytical expression for the wavevector modes of the MIM cavity was used (see eq 3-9). For the dielectric of the metal, the Drude model was used as before with the damping of the metal set to its intrinsic value under the classical model and set to the sum of the intrinsic and the Landau Damping induced damping rate calculated in the previous section under the Landau Damping model.

The mode volume was estimated geometrically. It was assumed that the mode will exist only in the gap between the two metals and will be negligible on the other surfaces and in free space. This assumption is valid due to the high confinement in the plasmonic

structures as well as the loss being dominated by materials losses as opposed to radiative losses. Within the gap, the field was assumed to be approximately uniform in the width direction. This is valid since the comparatively large width of the structure will prevent significant variations in that direction. Along its length the field was assumed to vary as $\propto \sin(\frac{\pi}{L}z)$, due to the fact we are analyzing the primary mode of the cavity. In the transverse height direction, the energy is assumed to be spread out over the mode length previously calculated for the MIM waveguide. These assumptions result in the following expression for the mode volume that can be computed just using the geometry and the mode length:

$$V = \frac{\int_V u_e(r)\,dr}{u_e(r_c)} = \frac{\int_0^L \int_0^W \int u_{1D,e}(y)\ \sin^2\left(\frac{\pi}{L}z\right) dzdxdy}{u_{1D,e}(y_0)}$$

$$= \int_0^L \sin^2\left(\frac{\pi}{L}z\right) dz \int_0^W dx \int \frac{u_{1D,e}(y)}{u_{1D,e}(y_0)} dy = \frac{L}{2} \cdot W \cdot M(G)$$

$$(4-3)$$

Where L and W are the length and the width of the cavity, and M is the mode length for the waveguide mode for the given gap thickness as calculated in the previous section.

From Q and V, the Purcell factor for the MIM cavities was computed using the following formula to provide a figure of merit for the cavity[29]:

$$F = \frac{3}{4\pi^2}\left(\frac{\lambda}{\sqrt{\varepsilon_g}}\right)^3 \frac{Q}{V} \qquad (4-4)$$

Finally, two possible uses for these MIM cavity were evaluated: enhancing the radiative spontaneous emission rates and achieving strong coupling between light and matter. The former is important for the realization of high rate single photon sources, one of the

biggest opportunities for quantum plasmonics [24]. The second is vital for a variety of quantum optics applications.

To understand the rate enhancement, the radiative spontaneous emission rate was considered. This differs from the Purcell Factor given above because the Purcell factor gives the total spontaneous emission (SE) rate and does not consider the proportion of the photons radiated out of the cavity versus absorbed by the metal. This radiated SE rate enhancement is given by the following equation [31]

$$\frac{\gamma_{SE}}{\gamma_0} = F\frac{\gamma_{rad}}{\gamma_{total}} \qquad (4-5)$$

where $\frac{\gamma_{SE}}{\gamma_0}$ is the radiated SE enhancement, γ_{rad} is the radiation rate, and γ_{total} is the total decay rate. The radiative rate can be written as [31]

$$\gamma_{rad} \propto \omega\frac{V}{\lambda} \qquad (4-6)$$

Thus, the resulting expression for the emission enhancement is:

$$\frac{\gamma_{SE}}{\gamma_0} \propto F\frac{V}{\lambda}\frac{\omega}{\gamma_{total}} = F\frac{V}{\lambda}Q \propto Q^2 \qquad (4-7)$$

The other possible application for plasmonic MIM nanocavities is to enter the strong coupling regime for light-matter interactions. This occurs when a photon is in the cavity long enough it is most likely to be reabsorbed, which can be written as [29]:

$$\frac{2g}{\kappa} = Q\sqrt{f\frac{\lambda^3}{V}}\sqrt{\frac{r_e}{2\pi\lambda}} > 1 \qquad (4-8)$$

Where *f is* the oscillator strength and r_e is the classical radius of the electron, and $\frac{2g}{\kappa}$ is proportional to the coupling of the cavity-emitter system divided by the optical losses in the cavity. In this work, in order to avoid any assumptions about the emitter, the terms related to the emitter were neglected and only the following expression was considered:

$$\frac{C}{L} = \frac{Q\lambda}{\sqrt{V}} \qquad (4-9)$$

Which we will call the coupling-loss ratio If the cavity parameters increase this expression, the cavity will be closer to entering the strong coupling regime regardless of what emitter is placed within it. It provides a tool to analyze how different parameters of cavity bring the cavity closer to entering the strong coupling regime both under classical models, and when Landau Damping is considered.

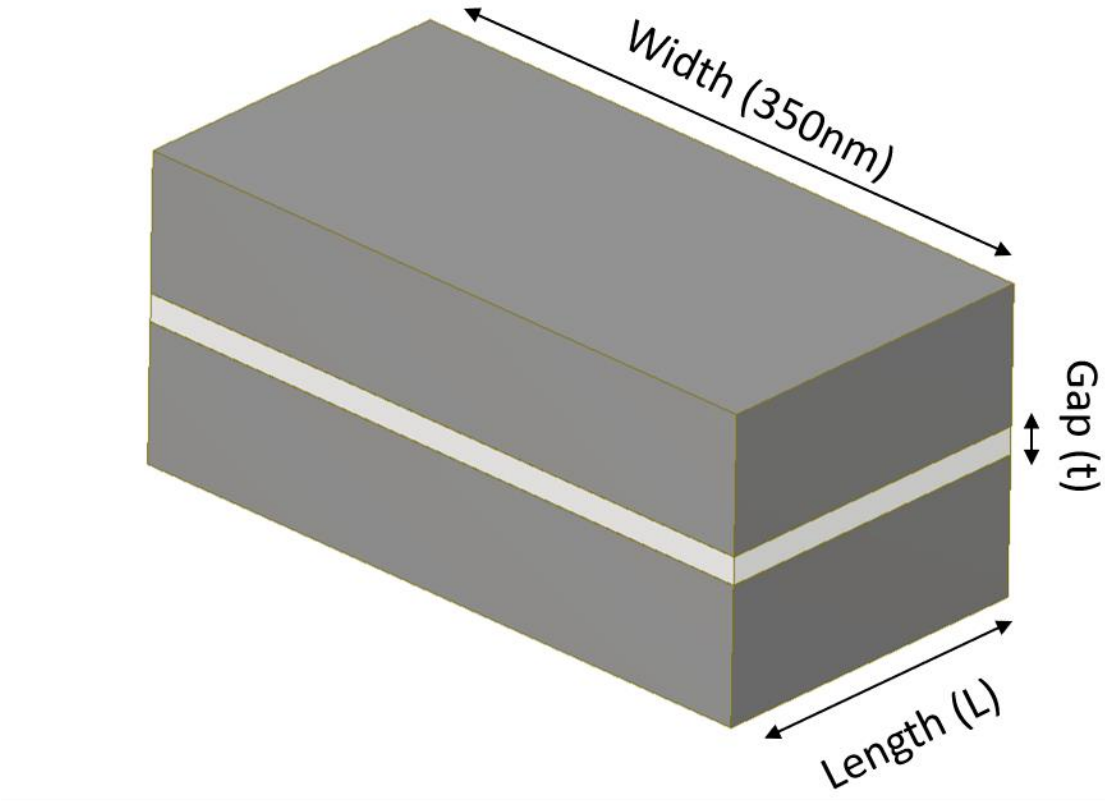

Figure 1: Diagram of constant-gap MIM Cavity. Diagram of the MIM cavity considered in this work consisting of two finite pieces of metal with length L and width of 350nm sandwiching an inner dielectric gap with constant thickness *t*. L was set such that the primary resonance occurred at the given gap size and design wavelength. Note that only the primary resonance in the gap along L was considered.

Chapter 5

EFFECTS OF LANDAU DAMPING IN MIM CAVITIES

In this section, the properties of the constant-gap MIM cavities formed through the truncation of an MIM waveguide are analyzed. Through use of both the Landau Damping and classical models, the effects of Landau Damping on performance under extreme confinement is analyzed.

It is found that Landau Damping does not affect the mode volume of these structures, but it does significant decrease the quality factor as the gap is shrunk. This large effect on Q leads to a variety of consequences for quantum optics applications through both decreasing the achievable radiated spontaneous emission rate and limiting the achievability of the strong coupling regime.

Performance of MIM Cavities with Decreasing Gap Sizes:

To get a sense of how Landau Damping impacts the performance of these MIM cavities, the cavity parameters for an MIM cavity consisting of an ideal metal under the Landau Damping model and Ag under both the classical and Landau models, were calculated using FEM simulations with an inner dielectric constant of 8 and a varying gap thickness *t*. (Figure 2). The varying gap size is particularly important for plasmonic cavity applications as decreasing the gap significantly increases the confinement. Under the classical model this would improve the performance and thus the gap could be decreased indefinitely until the desired performance is achieved.

The calculated quality factors show markedly different behavior between the classical and Landau Damping models (Figure 2a). Beyond the significant drop in Q when Landau Damping is taken into account, Q also continues to drop at small gaps unlike the constant Q seen in the classical simulations. Under the classical model, Q only changes slightly as it asymptomatically approaches its minimum value. This behavior was previously reported for similar MIM cavities in Ref [51] and is due to the cancelling out of the additional loss due to increased confinement and slower group velocity leading to the asymptotic quasi static limit. Moreover, this limit can be computed entirely from the material parameters through the following equation:

$$Q_{Quasi-Static} = \omega \frac{\frac{\partial \varepsilon_m'}{\partial \omega}}{2\varepsilon_m''} \qquad (5-1)$$

Where ω is the frequency of the mode, and ε_m' and ε_m'' are the real and imaginary parts respectively of the dielectric constant of the metal at the given wavelength. For the material parameters used in this work, the quasi-static Q is computed to be 74, which matches the classical simulations extremely well.

However, in the Landau Damping model, the Q decreases as the gap is further miniaturized far below the quasi-static limit, showing no asymptotic behavior. Due to Landau Damping, the loss in the material is a function of the confinement. Thus, as the gap is miniaturized, the confinement increases, and the loss increases with it. This leads to an increasing value for ε_m'' as the Landau Damping damping rate increases, causing the value for $Q_{Quasi-Static}$ to drop as the gap decreases as opposed to remaining constant.

To quantify this, under the Drude model we can write that:

$$\varepsilon_m'' = \frac{\omega_p^2}{\omega^3}\gamma_{LD} \qquad (5-2)$$

Where we assumed an ideal metal so that the only contribution to damping is the Landau Damping term. Then combining this with the expression for the Landau damping induced damping rate at high confinements and the expression for the quasi static quality factor (see eq 3-12 and 5-2)

$$Q_{Quasi-Static,LD} = \frac{2\omega^4}{3\omega_p^2}\left(\frac{\partial \varepsilon_m'}{\partial \omega}\right)\cdot\frac{\varepsilon_m' t}{v_f \varepsilon_g} \propto t \qquad (5-3)$$

Thus, at high confinements we conclude that Landau Damping causes the quality factor of plasmonic cavities to linearly decrease as the gap is decreased. This is not due the fact that the quasi-static limit is being violated. Instead since the material parameters are gap dependent the quasi-static limit becomes gap dependent as well, causing $Q \propto t$. This significant drop in Q will have important ramifications for the possible quantum optics applications of these devices. Note that at larger gap sizes, the Q deviates from linearity due to the non-unity reflection at the MIM-air interface.

The mode volume was calculated (Fig 1b). No significant change is seen between the classical and Landau Damping models. This is since Landau Damping does not affect the mode length, as seen in the previous section. However, V drops nonlinearly as the gap is decreased. To quantitatively understand the nonlinear drop in V versus gap, note that using equation 3-11, at small gaps the length of the cavity is given by:

$$L = \frac{\pi}{Re\big(k(G)\big)} = -\frac{\pi t \varepsilon_m'}{2\varepsilon_g} \propto t \qquad (5-4)$$

Empirically, M $\propto t$ as seen in the previous chapter. Thus, since W is constant, we conclude that V= $M \cdot L = \propto t^2$, so there is a quadratic drop in V as t decreases. This will have important ramifications for the behavior of the cavity for quantum optics applications.

The Purcell Factor was computed, giving an overall figure of merit for the cavity (Fig 1c). The ideal and Ag cavities under the LD model show an order of magnitude drop in the Purcell Factor as compared to the classical models, due to the Landau Damping induced losses. However, the Purcell Factor still increases as the gap is decreased. This is since V $\propto t^2$ but Q $\propto t$, so F$\propto \frac{Q}{V} \propto \frac{1}{t}$, so the nonlinear improvement in the mode volume outweighs the linear decrease in the quality factor. Thus, the main effect of Landau Damping on the Purcell Factor is a non-negligible drop, but the Purcell Factor will still increase as the gap is miniaturized up until tunneling sets in.

Very interesting behavior is seen for the two MIM cavity applications examined. First we study the possible spontaneous emission rate (rSE) enhancement in the MIM cavity (Fig 1d). The enhancement under the Landau Damping model is significantly lower than the enhancement under the classical model for Ag. This is naturally expected due to the higher losses introduced by Landau Damping. Moreover, whereas under the classical model, the achievable rate plateaus as the gap is miniaturized, the introduction of Landau Damping causes a significant decrease in rSE as the gap is further miniaturized even for non-ideal metals.

To explain this, notice that at high confinements, decreasing *V* no longer increases rSE due to the increase in Purcell Factor being cancelled out by a corresponding decrease in the rate of radiation. Thus, rSE fully depends on *Q*. Under the classical models, Q

asymptotically approaches the quasi-static limit, leading to little change and thus the rSE rate remains constant as the gap is miniaturized. However, with Landau Damping, the increasing damping with increased confinement causes Q to significantly decrease as the gap is miniaturized, leading to a decreased rSE rate. More quantitatively, it is known that for an ideal metal when Landau Damping is considered, $Q \propto t$, and $\frac{\gamma_{SE}}{\gamma_0} \propto Q^2 \propto t^2$, explaining the large decrease in rSE as the gap decreases. Previously researchers proposed to shrink the gap of plasmonic cavities to maximize the SE rate enhancement, but the analysis given here demonstrates that this will actually decrease performance below a certain gap size. Moreover, this further limits the maximum SE enhancement below previously computed limits.

The behavior of the coupling-loss ratio as the gap was miniaturized was then examined (Fig 1e). Beyond the drop in ratio between the classical and Landau Damping models expected due to the extra loss involved which on its own makes strong coupling more difficult to achieve, extremely different trends are observed. Traditionally, it has been thought that further miniaturization of plasmonic cavities would lead to higher confinements, eventually allowing the entering of the strong coupling regime. This interpretation is supported by the results under the classical model, which shows an extremely large increase in the coupling-loss ratio as the gap is miniaturized of over an order of magnitude. Under the Landau Damping model however, the ideal metal does not show a significant improvement as the gap is miniaturized below 10nm. The Ag cavity under the Landau Damping model does show some improvement, but much smaller than what is achieved under the classical model. This is an extreme consequence of Landau Damping.

Under the classical model, V decreases but Q remains constant as *t* is decreased, leading to an increase in the cavity-loss ratio that is seen in the calculations. When Landau Damping is taken into account, however, $Q \propto t$ and $V \propto t^2$, so both decrease. However, the strong coupling coefficient $\propto \frac{Q}{\sqrt{V}} \propto 1$. Thus the increased losses as the gap is miniaturized cancels out the increased confinement under the Landau Damping model, explaining why very little increase is seen. Note that at extremely small gaps some improvement is seen due to the breakdown of the assumptions used to derive the analytic expressions, but even these changes are quite modest. Therefore, we see that in rectangular MIM cavities, decreasing the gap size below 10nm does not improve the emitter coupling to loss ratio due to Landau Damping. Moreover, through the ideal metal, Landau Damping sets an upper bound on the maximum achievable ratio. To achieve strong coupling in MIM rectangular waveguides, the other design properties of the waveguide must be changed, such as the dielectric, wavelength, and emitter used, as opposed to the gap size or the material.

Effect of Wavelength on MIM Cavity Performance

The behavior of the cavity under different wavelengths was analyzed while the gap was fixed at 1nm (Fig 2). The Q factor shows a large qualitative change, as under the classical model it increases as the wavelength is shortened but under the Landau Damping model it slightly decreases as the wavelength is shortened (Fig 2a). Intuitively, this is since Landau Damping causes increased damping as the wavelength is shortened (see chapter 3) and that outweighs the classical increase in the quality factor leading to a net decrease. Mathematically, from eq 5-3, under the Landau Damping model at high confinements $Q \propto$

$\omega^4 \left(\frac{\partial \varepsilon_m'}{\partial \omega}\right) \cdot \varepsilon_m'$. From the Drude model, if the damping constant is small relative to the frequency then $\varepsilon_m' \propto \omega^{-2}$ and $\left(\frac{\partial \varepsilon_m'}{\partial \omega}\right) \propto \omega^{-3}$ so therefore $Q \propto \omega^4 \left(\frac{\partial \varepsilon_m'}{\partial \omega}\right) \cdot \varepsilon_m' \propto \omega^{-1}$, explaining the decrease at smaller wavelengths.

The mode volume, V, was calculated as before (Fig 2b). It decreases significantly as the wavelength is shortened due to the smaller wavelength leading to a shorter length necessary for the first resonance. At high confinements, $L \propto \varepsilon_m' \propto \omega^{-2}$ (see equation 5-4**)**. Although the mode length is also wavelength dependent, this dependence is small compared to the change in L and thus can be ignored, so we get that $V \propto L \propto \omega^{-2}$. Just as before, no significant change is seen for V between the Landau Damping and classical models due to no significant change to the mode length.

The Purcell factor was calculated (Fig 2c). As in the gap sweep calculations, its behavior is dominated by the change in behavior in Q between the classical and Landau Damping models. First the Purcell factor is significantly lower under the Landau Damping model, due to the significant drop in Q from the additional damping Moreover, it is observed that the Purcell Factor significantly drops as the wavelength is shortened under the Landau Damping model, whereas it remains constant under the local models. This is due to the increase in induced Landau damping at smaller wavelengths, causing a drop in Q, and thus a lower Purcell Factor

Finally, the effects of this on the two possible applications were calculated. The radiated emission enhancement was calculated (Fig 3d). Unlike the classical model, which shows a constant enhancement versus wavelength, there is a significant drop in the emission rate as the wavelength is decreased. This is explained rSE's dependence on Q, and thus the

drop in Q due to Landau Damping causes a significant drop in performance when the wavelength is decreased just like when the gap was decreased. Thus, like waveguides, decreasing the wavelength can help mitigate the effects of Landau Damping.

The calculated coupling-loss ratios (Fig 3e), show a small increase at larger wavelengths due to the decrease of the induced damping., To explain this, we note that the coupling-loss ratio $\propto \lambda \frac{Q}{\sqrt{V}} \propto \lambda$.. Thus using larger wavelengths is one method for achieving strong coupling with an MIM cavity.

Effect of Inner Dielectric on MIM Cavity Performance

Finally, the value of the dielectric index was varied as the gap was set to 1nm to understand how it impacted performance. Q decreases significantly as the inner dielectric constant is increased (Fig 4a). This is due to the increased damping at higher inner dielectric constants due to increased confinement, as described by equation 5-4 with $Q_{Quasi-Static,LD} \propto \varepsilon_g^{-1}$.

V also decreases sharply as the inner dielectric constant is increased (Fig 4b). This is since the higher index mode has a larger wavenumber, and thus a smaller length is required for a first order resonance. This is seen in eq 4-3 where $V \propto L \propto \varepsilon_g^{-1}$

The effects of the inner dielectric on the Purcell Factor are analyzed. It is seen that like under classical models, the MIM cavities' Purcell Factors decrease as the inner dielectric constant is increased (Fig 4c), albeit more sharply due to the increased damping at higher inner dielectrics effect on Q as discussed above.

The radiated spontaneous emission enhancement was considered (Fig 4d). rSE decreases much faster under the Landau Damping model than the classical model as the dielectric constant increases. Since the rate $\propto Q^{-2} \propto \varepsilon_g^{-2}$, explaining the large drop. Thus, the radiated spontaneous emission rate can be greatly enhanced through using a low inner dielectric constant

Finally, the coupling-loss ratio was considered (Fig 4e). Under the classical model, increasing the inner dielectric of the cavity allows the cavity to be further miniaturized, significantly improving the emitter-cavity coupling. However, under the Landau Damping model, it is seen that the coupling slightly decreases as the inner dielectric constant increases. This is due to the additional damping at higher dielectric values outweighing the gain in miniaturization. Mathematically, the coupling $\propto \frac{Q}{\sqrt{V}} \propto \varepsilon_g^{-1/2}$ under the Landau Damping model, showing why there is a decrease albeit a slow one. Thus, changing the inner dielectric of a cavity does not significantly improve the ability to achieve strong coupling.

Thus, except for strong coupling, the properties of MIM cavities can be improved through decreasing the inner dielectric constant.

Discussion:

The introduction of Landau Damping leads to much more serious consequences for MIM cavities than for MIM waveguides. The additional damping significantly impacts Q, with detrimental ramifications. Three important aspects emerge. 1. Landau Damping causes a significant drop in Q as compared to the classical model, leading to orders of magnitude drops in the radiated spontaneous emission rates and cavity-emitter coupling

coefficients. 2. Like in the waveguide case, Landau Damping introduces damping into an ideal metal, which thus sets a maximum achievable Q, and therefore a maximum achievable radiated spontaneous emission enhancement and coupling-loss ratio for a given cavity geometry. 3. The increase of Landau Damping with decreasing gap size completely changes the trends of radiated spontaneous emission enhancement and coupling-loss ratio as the gap decreases. In both cases it prevents increasing performance through further miniaturization of the gap. The impact of these three points will now be discussed with regards to the two quantum optics applications considered.

Using plasmonic cavities to enhance the radiated spontaneous emission rate of single photon sources in one area where plasmonics is expected to excel. Plasmonic losses are not detrimental for this application, and it has been theoretically shown that plasmonics can achieve much larger rate enhancements than is possible with purely dielectric structures [31]. However, the above analysis demonstrates that Landau Damping severely limits this possibility. First the additional damping severely decreases the emission enhancement limiting the performance. More interestingly, Landau Damping causes the radiated spontaneous emission rate to actually drop as the gap is further miniaturized. This has two important ramifications. First, it was previously thought that miniaturizing the gap further should always increase the emission rate, but this analysis shows that not to be the case. Thus blindly fabricating smaller and smaller gaps to increase the rate enhancement will not work as previously thought, and these devices will require more careful engineering. Second it causes the maximum emission rate to be achieved at a relatively large gap size (above 10nm for the cavity considered in this work) with a comparatively lower

spontaneous emission rate, limiting the maximum achievable emission rate to below what was previously thought.

The effects of Landau Damping on achieving strong coupling with MIM cavity structures are equally severe. Below certain gap sizes, decreasing the gap further does not bring the system significantly closer to the strong coupling regime under the Landau Damping model. This effectively places a restriction on the minimum gap that can be used, below which no benefit will be gained. It also limits which systems strong coupling is theoretically achievable with a given emitter/plasmonic cavity combo, as unlike under classical models where the gap could be shrunk almost indefinitely until strong coupling is achieved, under the Landau Damping model no benefit is gained. Moreover, the introduction of losses into the ideal metal means that even improving the material will lead to only a marginal improvement over Ag. This decreases the possibility of many plasmonic systems achieving strong coupling.

Like in the waveguide case, the effects of Landau Damping can be minimized through using larger wavelengths and lower index materials for the inner dielectric. However as in many quantum optics applications these are not variables that are easily controlled, this is not as practical.

Finally, the limitations of the analysis performed in this section needs to be discussed. First it should be noted again that the simulations performed at this section and the associated analytical analysis assumed small gap sizes. At larger gap sizes, there is increased transmission at the MIM-air end interface of the cavity and that will likely overshadow the effects of Landau Damping. In addition, for a non-ideal metal with an intrinsic damping rate, at larger gap sizes when the induced damping rate is significantly smaller than the intrinsic

rate the cavity will behave as it would under classical models. Thus, the above analysis only applies to highly confined MIM cavities, with gaps less than 10nm.

Second, we only considered the first order resonance of a constant-gap rectangular cuboid cavity. Although this closely resembles a cubic cavity with the same side lengths formed by cubic nanoparticles, it differs in its length, as the cavities considered here had its length set such that the first order resonance occurred at the design wavelength. In addition, higher order resonances were never considered, and their behavior may differ as well. Thus, other cavities with similar shapes may behave slightly differently, although the general trends are expected to be similar.

Finally, completely different nanoplasmonic cavity geometries were not considered also are not expected to follow the same trends as the cavities in this work. In particular, the nanosphere on mirror cavity has been used to demonstrate strong coupling in a plasmonic platform and has been argued to be superior for these sorts of applications [35, 54]. However, early work has shown that Landau Damping causes an increase in its mode volume which is very different from the cavity considered in this work [47]. Thus, the results in this work cannot be extended to that platform and additional work is required to understand the effects of Landau Damping in that, as well as other, plasmonic platforms.

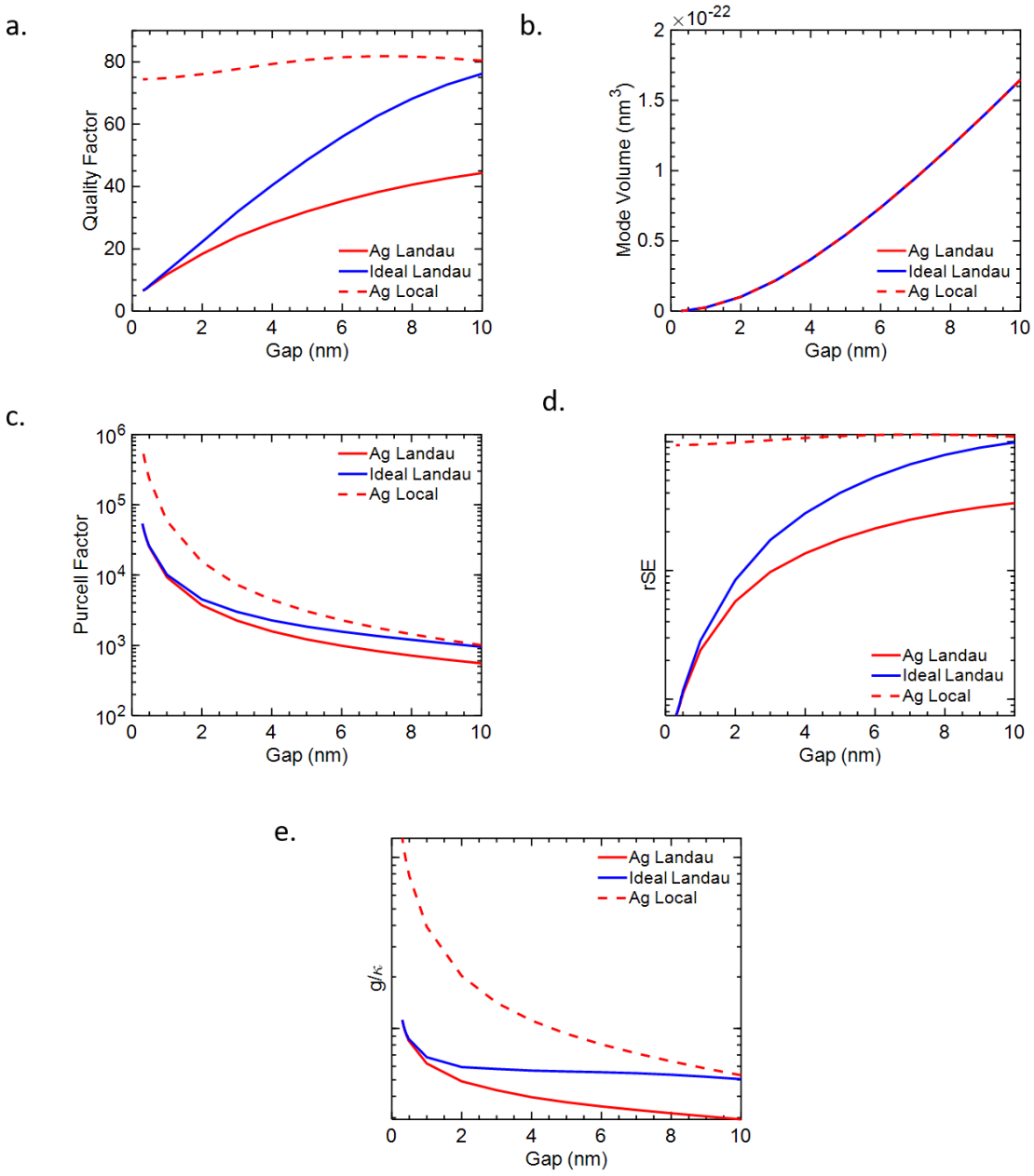

Figure 1: Parameters of MIM Cavity versus Gap. a. The Q versus the gap size, showing a linear decrease and a significant drop under the Landau Damping model as opposed to the classical model which shows minimal change. b. The mode volume versus gap size, showing a nonlinear decrease as the gap size is decreased and no change between the different models. c. The Purcell Factor versus gap size, showing an order of

magnitude drop between the classical and Landau Damping models, but a similar trend of increasing as the gap is smaller. d. The radiated spontaneous emission enhancement versus gap size, showing a significant drop as the gap size is decreased under the Landau Damping model, which is impactful for single photon sources. e. The coupling-loss ratio for strong coupling versus gap size, showing only a slight increase with decreasing gap size under the Landau Damping model, as opposed to a significant increase under classical models.

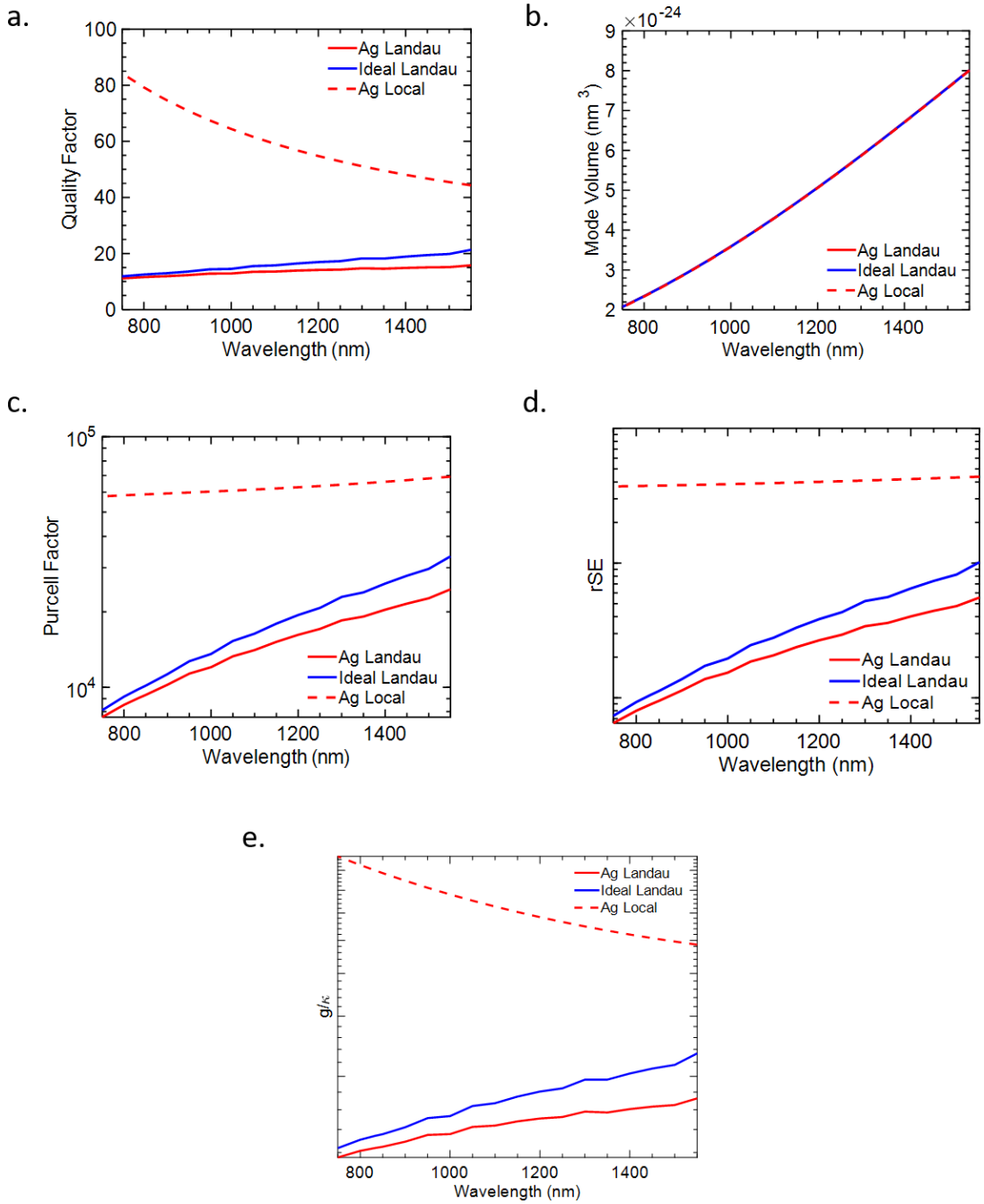

Figure 2: Parameters of MIM Cavity versus Wavelength. a. The Q versus the wavelength, showing an improvement as the wavelength increases under the Landau Damping model but the opposite under the classical model. b The mode volume versus wavelength, showing an increase versus wavelength but no significant difference

between the two models. c. The Purcell Factor versus wavelength showing an improvement as the wavelength increases. d. The radiated spontaneous emission rate enhancement versus wavelength, showing a noticeable improvement as the wavelength is increased under the Landau Damping model but not under the classical model. e. The coupling-loss ratio versus wavelength, showing a slight improvement with increasing the wavelength under the Landau Damping model.

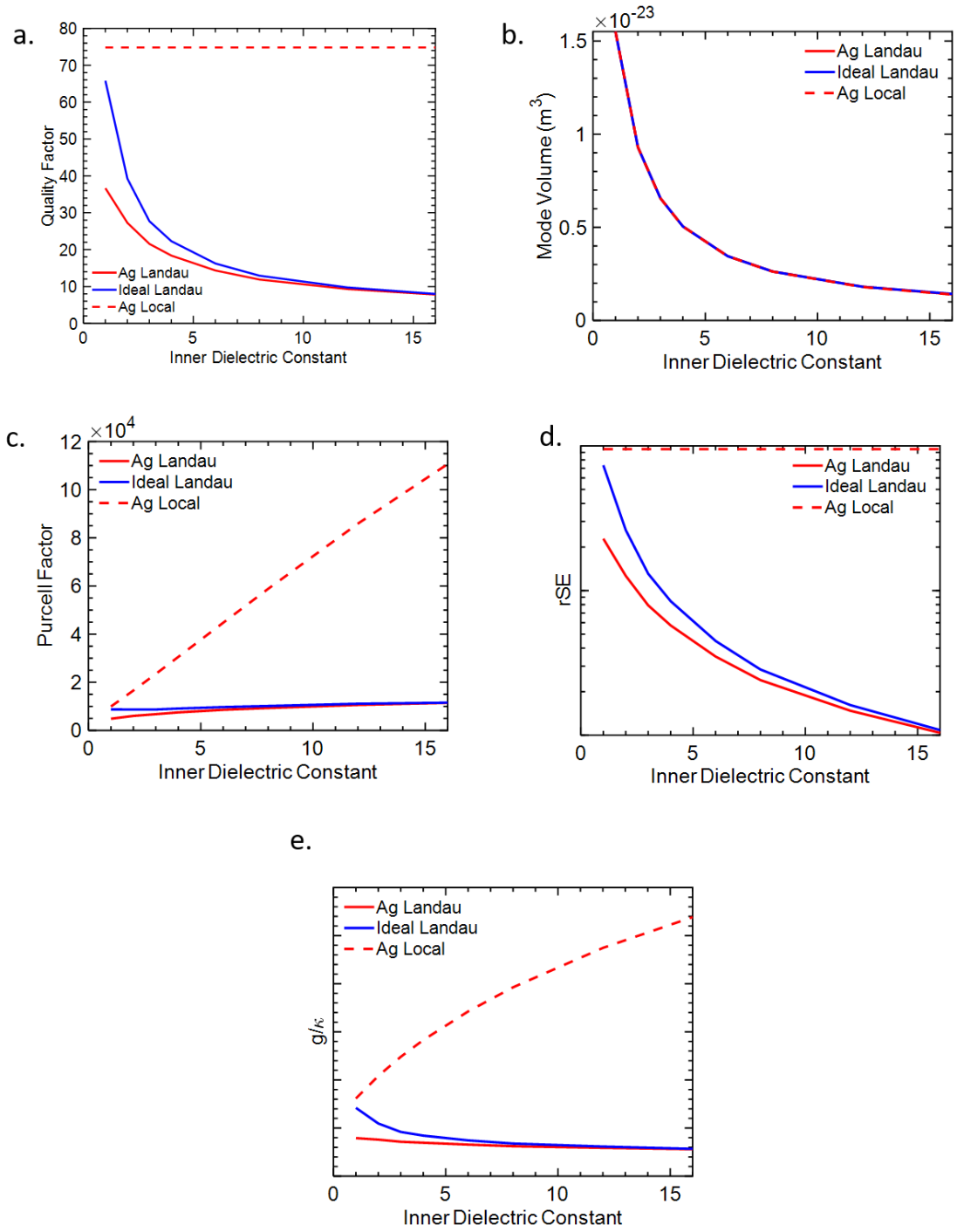

Figure 3: Parameters of MIM Cavity versus Inner Dielectric Constant . a. The Q versus the inner dielectric, showing a significant decrease under the Landau Damping model due to the increasing induced loss. b. The mode volume versus inner dielectric

showing no change between the Landau and classical models and showing a decrease with increasing dielectric constants. c. The Purcell Factor versus inner dielectric, showing a decrease with increasing dielectric constant that is increased due to Landau Damping. d. The radiated spontaneous emission enhancement versus inner dielectric, showing that Landau Damping causes a much larger drop in the enhancement as the inner dielectric constant is increased due to increased damping. e. The coupling-loss ratio versus inner dielectric, showing that Landau Damping causes a slight decrease in the coupling as the inner dielectric is increased which is not expected under the classical model.

Chapter 6

CONCLUSION

In this work we analyze the effects of Landau Damping in plasmonic MIM waveguides and cavities. In waveguides, it is found that the introduction of damping does not significantly affect the mode length, ensuring that it does not limit the achievable confinement which is thus limited by tunneling (See Appendix B). However, Landau Damping does significantly decrease the propagation length and limits the maximum achievable propagation length in a bulk metal. These results limit the potential for highly compact integrated MIM waveguides, but nanofocusing for molecular probing is mostly unaffected.

In MIM cavities with a constant gap thickness, the mode volume is unaffected whereas the quality factor is decreased due to the introduction of Landau Damping, Moreover, the quality factor continues to decrease as the gap is miniaturized. This causes the radiated spontaneous emission rate to actually decrease as the gap is decreased past a certain point. This limits the emission rate enhancement achievable for single photon sources. Moreover, the coupling-loss ratio in the cavity does not significantly increase as the gap is decreased anymore, limiting the achievability of strong coupling for certain emitter-cavity pairs. In both cases, it was found that through using a larger wavelength and a lower inner dielectric constant, these effects could be minimized

Thus, the work fully explores the effects of Landau Damping in MIM platforms. In terms of future work, the next important step is to experimentally verify the above

predictions. We have designed an experiment using self-assembled nanocube cavities that would provide conclusive evidence for the existence of effects discussed in this thesis (see Appendix A).

Beyond that, additional theoretical points of Landau Damping need to be investigated. First the above analysis should be extended to other cavity geometries, such the commonly used Nanoparticle on Mirror geometry which will likely have a different response to the introduced damping. Second, the effects of plasmonic Landau Damping in 2D materials still needs to be theoretically and experimentally explored to see if it provides an avenue for low-loss gap plasmonics.

Finally, device design and experimental work needs to be undertaken to engineer around the limitations of Landau Damping. As discovered in this work, Landau Damping is extremely harmful to the future of integrated plasmonic waveguides and cavity systems. However, through a combination of using a larger wavelength and low inner dielectric and clever engineering through combining plasmonic systems with dielectric or active systems, it can be possible to mitigate the effects of Landau Damping. This clever engineering combined with the knowledge developed in this thesis will be vital in the realization of practical nanogap plasmonic systems.

REFERENCES

1. Thomson, D., et al., *Roadmap on silicon photonics.* Journal of Optics, 2016. **18**(7): p. 073003.
2. Wang, C., et al., *Integrated lithium niobate electro-optic modulators operating at CMOS-compatible voltages.* Nature, 2018. **562**(7725): p. 101-104.
3. Reed, G.T., et al., *Silicon optical modulators.* Nature Photonics, 2010. **4**: p. 518.
4. Shi, X., D.V. Verschueren, and C. Dekker, *Active Delivery of Single DNA Molecules into a Plasmonic Nanopore for Label-Free Optical Sensing.* Nano Letters, 2018. **18**(12): p. 8003-8010.
5. Taylor, A.B. and P. Zijlstra, *Single-Molecule Plasmon Sensing: Current Status and Future Prospects.* ACS Sensors, 2017. **2**(8): p. 1103-1122.
6. Yang, D., et al., *Glucose Sensing Using Surface-Enhanced Raman-Mode Constraining.* Analytical Chemistry, 2018. **90**(24): p. 14269-14278.
7. Gooding, J.J. and K. Gaus, *Single-Molecule Sensors: Challenges and Opportunities for Quantitative Analysis.* Angewandte Chemie International Edition, 2016. **55**(38): p. 11354-11366.
8. Aharonovich, I., D. Englund, and M. Toth, *Solid-state single-photon emitters.* Nature Photonics, 2016. **10**: p. 631.
9. O'Brien, J.L., A. Furusawa, and J. Vučković, *Photonic quantum technologies.* Nature Photonics, 2009. **3**: p. 687.
10. Sipahigil, A., et al., *An integrated diamond nanophotonics platform for quantum-optical networks.* Science, 2016. **354**(6314): p. 847.
11. Maier, S.A., *Plasmonics: Fundamentals and Applications*. 2007, New York: Springer.

12. Maier, S.A., *Plasmonic field enhancement and SERS in the effective mode volume picture.* Optics Express, 2006. **14**(5): p. 1957-1964.

13. Prade, B., J.Y. Vinet, and A. Mysyrowicz, *Guided optical waves in planar heterostructures with negative dielectric constant.* Physical Review B, 1991. **44**(24): p. 13556-13572.

14. Choo, H., et al., *Nanofocusing in a metal–insulator–metal gap plasmon waveguide with a three-dimensional linear taper.* Nature Photonics, 2012. **6**: p. 838.

15. Fang, Y. and M. Sun, *Nanoplasmonic waveguides: towards applications in integrated nanophotonic circuits.* Light: Science &Amp; Applications, 2015. **4**: p. e294.

16. Ho, Y.-L., et al., *On-Chip Monolithically Fabricated Plasmonic-Waveguide Nanolaser.* Nano Letters, 2018. **18**(12): p. 7769-7776.

17. Kneipp, K., et al., *Single Molecule Detection Using Surface-Enhanced Raman Scattering (SERS).* Physical Review Letters, 1997. **78**(9): p. 1667-1670.

18. Nie, S. and S.R. Emory, *Probing Single Molecules and Single Nanoparticles by Surface-Enhanced Raman Scattering.* Science, 1997. **275**(5303): p. 1102-1106.

19. Xu, H., et al., *Spectroscopy of Single Hemoglobin Molecules by Surface Enhanced Raman Scattering.* Physical Review Letters, 1999. **83**(21): p. 4357-4360.

20. Kildishev, A.V., A. Boltasseva, and V.M. Shalaev, *Planar Photonics with Metasurfaces.* Science, 2013. **339**(6125): p. 1232009.

21. Yu, N. and F. Capasso, *Flat optics with designer metasurfaces.* Nature Materials, 2014. **13**: p. 139.

22. Yu, N., et al., *Light Propagation with Phase Discontinuities: Generalized Laws of Reflection and Refraction.* Science, 2011. **334**(6054): p. 333-337.

23. Bogdanov, S.I., et al., *Ultrabright Room-Temperature Sub-Nanosecond Emission from Single Nitrogen-Vacancy Centers Coupled to Nanopatch Antennas.* Nano Letters, 2018. **18**(8): p. 4837-4844.

24. Bozhevolnyi, S.I. and J.B. Khurgin, *The case for quantum plasmonics.* Nature Photonics, 2017. **11**: p. 398.

25. Andersen, S.K.H., S. Kumar, and S.I. Bozhevolnyi, *Ultrabright Linearly Polarized Photon Generation from a Nitrogen Vacancy Center in a Nanocube Dimer Antenna.* Nano Letters, 2017. **17**(6): p. 3889-3895.

26. Haurylau, M., et al., *On-Chip Optical Interconnect Roadmap: Challenges and Critical Directions.* IEEE Journal of Selected Topics in Quantum Electronics, 2006. **12**(6): p. 1699-1705.

27. Betzig, E. and R.J. Chichester, *Single Molecules Observed by Near-Field Scanning Optical Microscopy.* Science, 1993. **262**(5138): p. 1422-1425.

28. Trautman, J.K., et al., *Near-field spectroscopy of single molecules at room temperature.* Nature, 1994. **369**(6475): p. 40-42.

29. Marquier, F., C. Sauvan, and J.-J. Greffet, *Revisiting Quantum Optics with Surface Plasmons and Plasmonic Resonators.* ACS Photonics, 2017. **4**(9): p. 2091-2101.

30. Purcell, E.M., *Spontaneous emission probabilities at radio frequencies.* Physical Review, 1946. **69**.

31. Bozhevolnyi, S.I. and J.B. Khurgin, *Fundamental limitations in spontaneous emission rate of single-photon sources.* Optica, 2016. **3**(12): p. 1418-1421.

32. Fernández-Domínguez, A.I., S.I. Bozhevolnyi, and N.A. Mortensen, *Plasmon-Enhanced Generation of Nonclassical Light.* ACS Photonics, 2018. **5**(9): p. 3447-3451.

33. Walther, H., et al., *Cavity quantum electrodynamics.* Reports on Progress in Physics, 2006. **69**(5): p. 1325-1382.

34. Kleemann, M.-E., et al., *Strong-coupling of WSe2 in ultra-compact plasmonic nanocavities at room temperature.* Nature Communications, 2017. **8**(1): p. 1296.

35. Chikkaraddy, R., et al., *Single-molecule strong coupling at room temperature in plasmonic nanocavities.* Nature, 2016. **535**: p. 127.

36. Ojambati, O.S., et al., *Quantum electrodynamics at room temperature coupling a single vibrating molecule with a plasmonic nanocavity.* Nature Communications, 2019. **10**(1): p. 1049.

37. Leng, H., et al., *Strong coupling and induced transparency at room temperature with single quantum dots and gap plasmons.* Nature Communications, 2018. **9**(1): p. 4012.

38. Zhu, W., et al., *Quantum mechanical effects in plasmonic structures with subnanometre gaps.* Nature Communications, 2016. **7**: p. 11495.

39. Esteban, R., et al., *Bridging quantum and classical plasmonics with a quantum-corrected model.* Nature Communications, 2012. **3**: p. 825.

40. Zhu, W. and K.B. Crozier, *Quantum mechanical limit to plasmonic enhancement as observed by surface-enhanced Raman scattering.* Nature Communications, 2014. **5**: p. 5228.

41. Savage, K.J., et al., *Revealing the quantum regime in tunnelling plasmonics.* Nature, 2012. **491**: p. 574.

42. Tan, S.F., et al., *Quantum Plasmon Resonances Controlled by Molecular Tunnel Junctions.* Science, 2014. **343**(6178): p. 1496-1499.

43. Barton, G., *Some surface effects in the hydrodynamic model of metals.* Reports on Progress in Physics, 1979. **42**(6): p. 963-1016.

44. Dong, T., X. Ma, and R. Mittra, *Optical response in subnanometer gaps due to nonlocal response and quantum tunneling.* Applied Physics Letters, 2012. **101**(23): p. 233111.

45. Mortensen, N.A., et al., *A generalized non-local optical response theory for plasmonic nanostructures.* Nature Communications, 2014. **5**: p. 3809.

46. Khurgin, J.B., *Ultimate limit of field confinement by surface plasmon polaritons.* Faraday Discussions, 2015. **178**(0): p. 109-122.

47. Khurgin, J., et al., *Landau Damping and Limit to Field Confinement and Enhancement in Plasmonic Dimers.* ACS Photonics, 2017. **4**(11): p. 2871-2880.

48. Herrera, L.J.M., et al., *Determination of plasma frequency, damping constant, and size distribution from the complex dielectric function of noble metal nanoparticles.* Journal of Applied Physics, 2014. **116**(23): p. 233105.

49. Jin, J.-M., *Theory and Computation of Electromagnetic Fields*. 2010: John Wiley & Sons, Inc.

50. Ruppin, R., *Electromagnetic energy density in a dispersive and absorptive material.* Physics Letters A, 2002. **299**(2): p. 309-312.

51. Yang, J., et al., *Ultrasmall metal-insulator-metal nanoresonators: impact of slow-wave effects on the quality factor.* Optics Express, 2012. **20**(15): p. 16880-16891.

52. Baumberg, J.J., et al., *Extreme nanophotonics from ultrathin metallic gaps.* Nature Materials, 2019.

53. Alcaraz Iranzo, D., et al., *Probing the ultimate plasmon confinement limits with a van der Waals heterostructure.* Science, 2018. **360**(6386): p. 291-295.

54. Chikkaraddy, R., et al., *How Ultranarrow Gap Symmetries Control Plasmonic Nanocavity Modes: From Cubes to Spheres in the Nanoparticle-on-Mirror.* ACS Photonics, 2017. **4**(3): p. 469-475.

Appendix A

PROPOSED EXPERIMENTAL VERIFICATION

Having determined the effects of Landau Damping on MIM plasmonic devices, the next step is to provide experimental verification that these effects do in fact occur. Landau Damping has previously been fit to experimental results for other plasmonic platforms, such as dimer platforms, explaining the peak broadening. However, it has yet to be directly observed in MIM cubic structures.

We propose to fabricate and measure MIM cubic cavities such as those discussed in the last chapter. The quality factor of the resonances can be measured, and through seeing if the trend in quality factor better matches that of the classical model or Landau model, experimental evidence will be provided for Landau Damping in this platform. In addition, since the limiting effects on the performance on the plasmonic cavities for quantum optics applications as determined in the previous section are due to the trends in the quality factor as the cavities are miniaturized, this will provide evidence for the detrimental effects of Landau Damping.

Experimental Design

We propose to use self-assembled nanocubes to form MIM cavities. To isolate the MIM gap modes, the transmission of the cavity will be measured either in free space or using an NSOM probe. Through this, the Qs of the different modes at different wavelengths and

different gap sizes can be analyzed to show the trends in Q due to Landau Damping. Each aspect will now be discussed in detail.

A pre-synthesized solution of Au nanocubes will be taken and dried on a glass slide. The drying will cause the nanocubes to agglomerate due to Van der Walls interactions. The density of the solution will be controlled so that large monolayers of cube aggregates will be formed.

To control the gap size of these monolayers, the surface coating of the Au nanocubes will be changed to change the gap size (Fig SA1a). Due to the Van der Walls interactions drawing the cubes together, the surface coating is what determines the gap size. Thus by changing the surface coating, different gaps can be fabricated. These nanocube arrays will be illuminated from the top. Due to their finite thickness, they act as MIM cavities similar to the ones considered in the previous chapter and thus showing similar trends in Q which can be observed. It should be noted that the proposed cavities have one major difference in that the cavities in the previous section had a thickness set such that the primary resonance occurred at the design wavelength whereas these nanocube cavities have a set thickness already that cannot be tuned. Thus, instead of just measuring the primary resonance, higher order resonances will be measured to observe the effects of Landau Damping. A picture of a monolayer of nanocubes formed using the above method is shown in Fig SA1b

To measure the Q of the modes of the cavities, a transmission measurement will be performed. The peaks in the transmission spectrum will correspond with different modes and the quality factor can then be extracted from the linewidth. To measure the transmission, either the freespace setup shown in Fig SA1c or an NSOM near field measurement shown in Fig 1d can be utilized. The advantage of the free space setup is that it is much simpler,

potentially possible in a standard microscope, at the cost of selectivity and signal. The NSOM setup is much more complex, but can gather a larger signal, and has the added advantage that it can measure individual dimers whereas the freespace setup can only measure diffraction limited spots. Thus, depending on whether the formed monolayers are at least as large as a diffraction limited spot will determine whether an NSOM measurement is necessary or if a freespace measurement will suffice. Once the transmission spectrum is measured, curves can be fit to it to extract the peak width and from that calculate the quality factors.

Simulations:

The transmission spectrum of the MIM cavities were simulated with FDTD software under the classical model and Landau Damping model. This was done for two reasons: to see if the differences in the Q factor predicted between the classical and Landau Damping model are big enough to measure and to see what exactly those differences are. The second point in particular is important, because the cavities fabricated experimentally are different than those considered theoretically in the previous chapter, so it has to be verified the same trends exist.

The transmission spectrums are shown in Figure SA2a/b considering a gap size of 2nm and a gap size of 5nm.Qualitatively, it is observed that the Landau damping curves are a bit broader, especially with the 2nm gap at small wavelengths.

To quantify this, the quality factors were calculated from the transmission spectrum through curve fitting (Figure SAs2c/d). From this, it is observed that there is a big discrepancy at 2nm at low wavelengths between the local and Landau models. At 2nm, it is

clearly observed that under the Landau Damping model, the quality factor decreases as the wavelength is decreased whereas the opposite behavior is observed under the classical model. Not only does this provide an experimentally observable measurement, it also is the same trend observed in the previous chapter verifying that many trends cross over to other types of cavities. Notice that under the Landau model the quality factor also drops at low wavelengths between a gap of 5nm and 2nm, whereas under the classical model it stays more or less the same, providing another observable. In addition, if Ag is used instead of Au these effects will be even more pronounced due to the lower intrinsic damping of Ag.

Thus, through measuring Au nanocube cavities with two gaps of 2nm and 5nm, the accuracy of the Landau Damping model and its predictions can be verified.

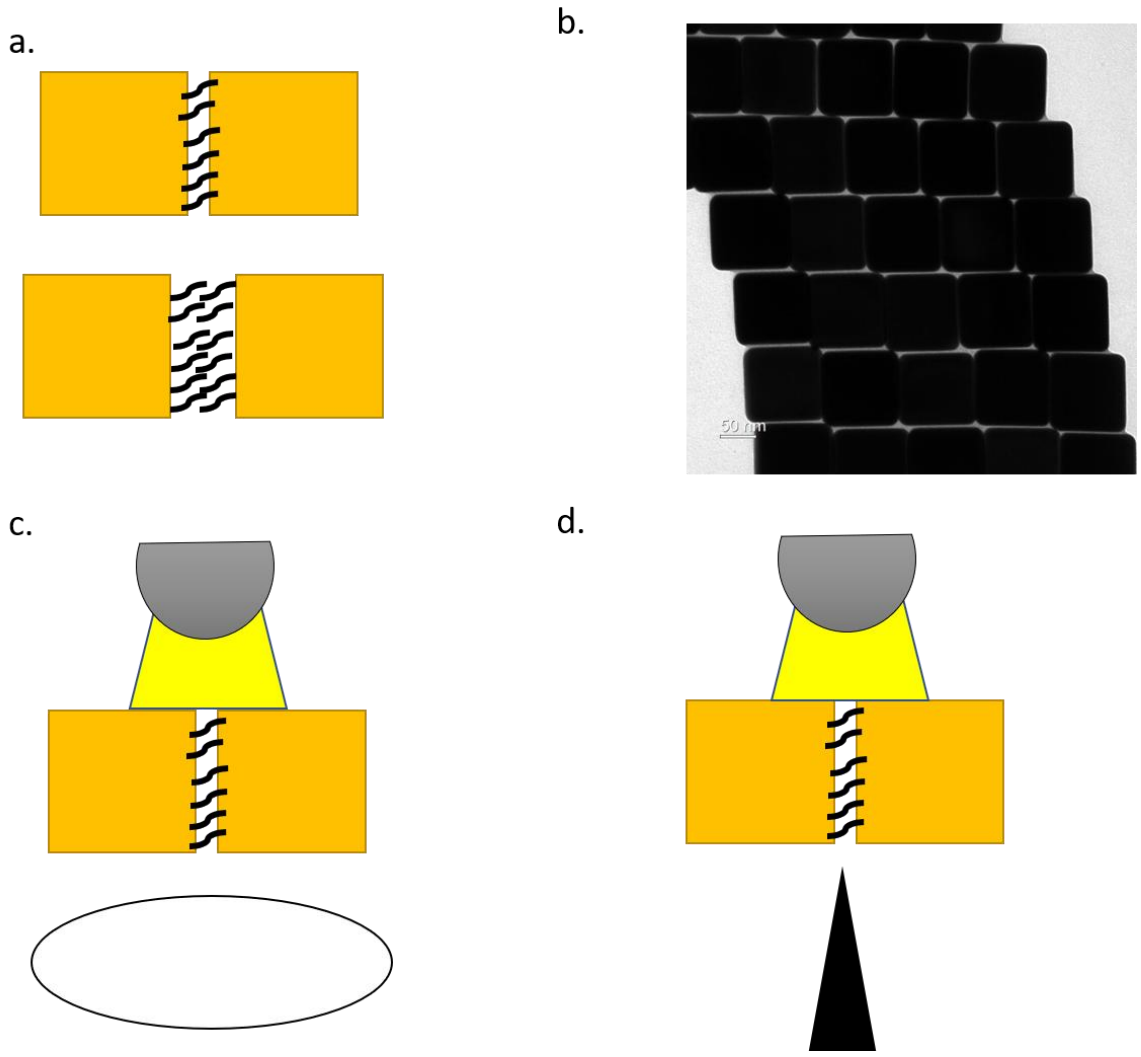

Figure SA1: Experimental Design . a. The fabrication of MIM cavity structures with variable gaps. The cavities are created through self-assembled nanocubes brought together through Van der Walls interactions. The gap is defined by the functionalization of the cube's surface, which can be altered to achieve different gap sizes. b. A TEM image of Au nanocubes that can be used for this purpose. c. Diagram of a freespace measurement setup to measure the transmission of the MIM cavity modes. The cavity is illuminated by a broadband source (top) and the light is collected by a lens on the other side which is then fed into a spectrometer. d. Diagram of a near field transmission

measurement setup, which is the same as the previous one except the lens is replaced by a metal coated fiber for NSOM transmission measurements.

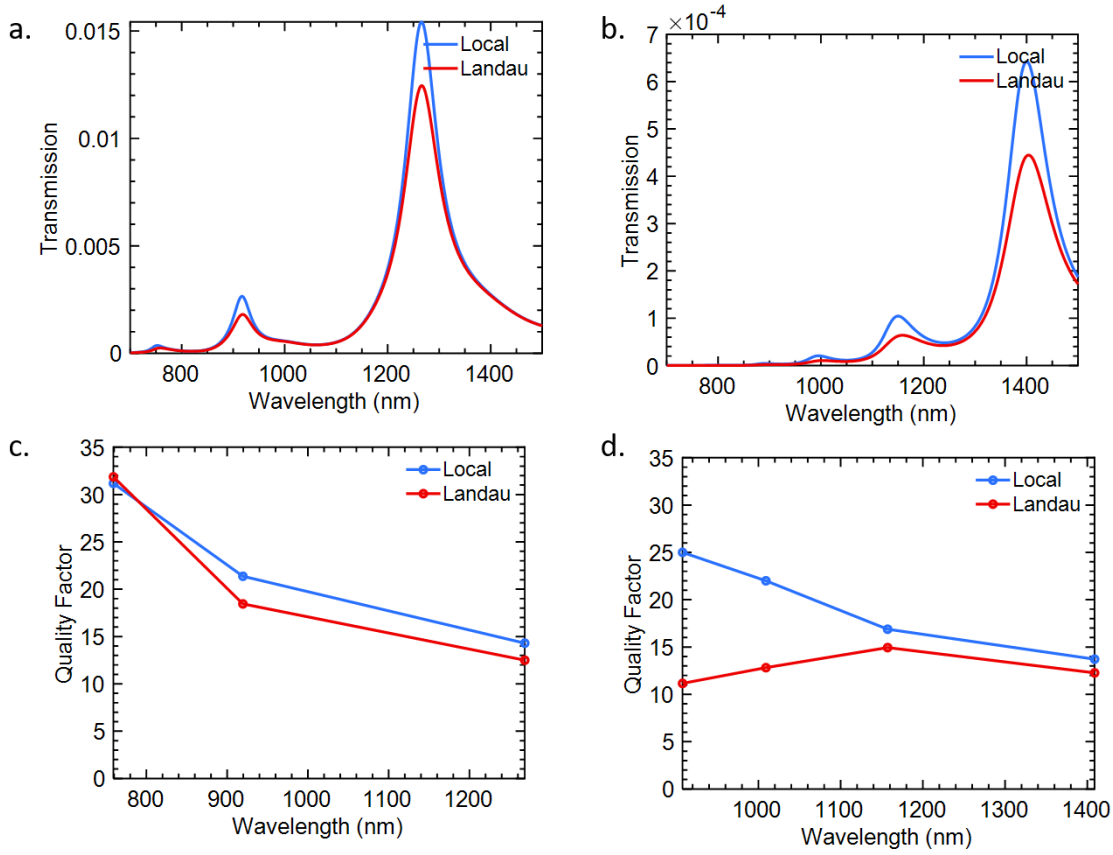

Figure SA2: Experimental Simulations a/b. The transmission spectrum of the MIM cubic cavities with gaps of 5nm (a) and 2nm (b) under the classical and Landau Damping models. The introduction of Landau Damping is seen to broaden the resonances shown by the transmission peaks. c/d. The quality factors extracted from the transmission spectrums at 5nm (c) and 2nm (d). It is seen that under the Landau Damping model, at 5nm the quality factor increases with decreasing wavelength whereas at 1nm the quality factor decreases with decreasing wavelength due to the introduction of larger damping. This provides an experimentally measurable outcome that can be used to further test the validity of the Landau Damping theory and provide evidence for the theoretical results determined in this work.

Appendix B

PERFORMANCE OF MIM WAVEGUIDES IN C-BAND

In the results from the MIM waveguide presented in chapter 3, the wavelength was set to 850nm except for the wavelength sweep, corresponding with the 850-band fiber band for integrated photonics applications. However, it is also possible for MIM waveguides to be used in the C-band (1550nm). Beyond the advantage of being able to use the fiber optic technology developed for the C-band, it has the added advantage that the Landau Damping induced damping rate is smaller at 1550nm as opposed to 850nm. Thus, better optimal performance can be expected, and it is important to provide numerical simulation results for MIM waveguides in the C-Band.

The properties of the MIM waveguide for an incident freespace wavelength of 1550nm was simulated as done in Chapter 3 (Fig SB1). Although qualitatively the same behavior is observed as with the incidence wavelength at 850nm, the induced damping rate was three times lower than earlier (Fig SB1a). This results in a significantly improved propagation length, even still being around 1 micron at a gap of 1nm in the ideal case. The difference in the propagation length s quite large, with the ideal metal having a propagation length of almost 3 microns (Fig SB1c). Thus, by operating the waveguides in the C-band, the effects of Landau Damping can be significantly decreasing, improving performance, and the data provided in this section can be used to more precisely consider possible C-band MIM systems.

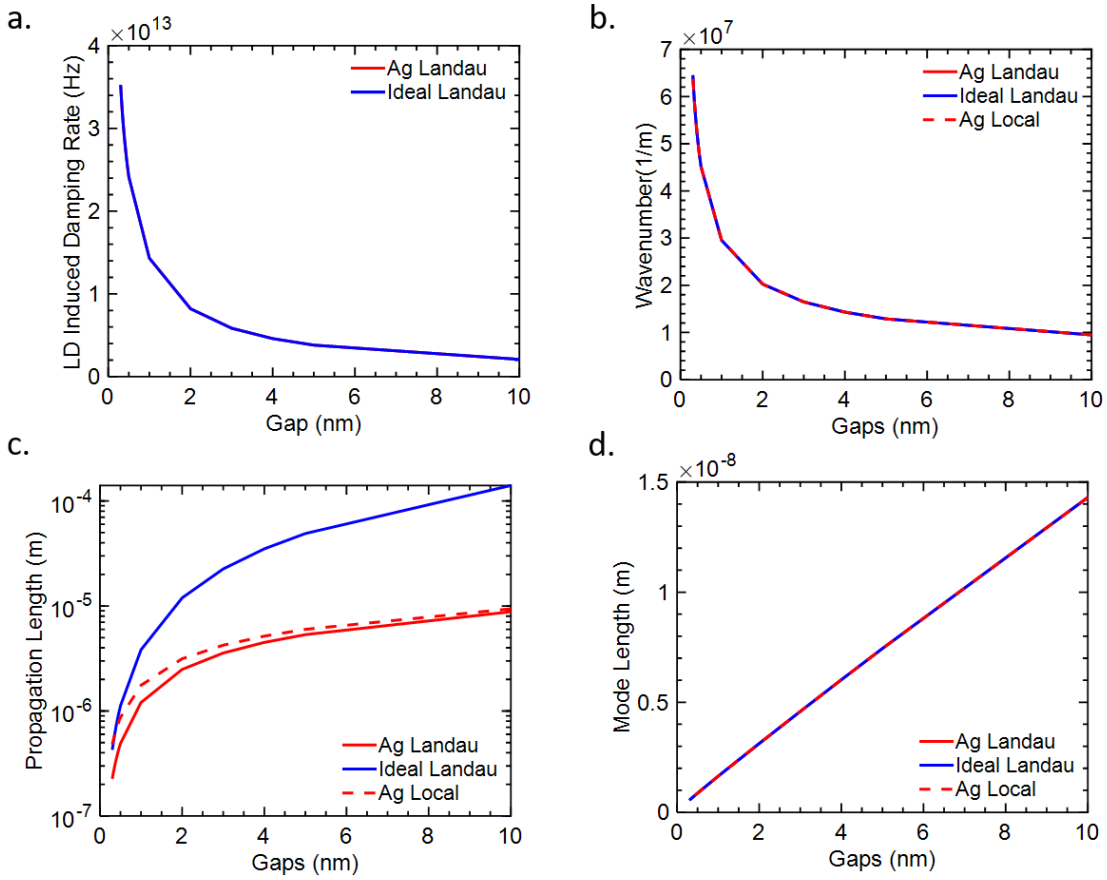

Figure SB1. Properties of the MIM waveguide versus gap thickness in the C-band. a. The induced Landau damping rate simulated for an Ag and an ideal metal waveguide as a function of gap thickness (curves are overlapped) as well as calculated. The damping rate significantly increases as the gap is miniaturized, but the rate is significantly lower than with an incident wavelength of 850nm. b. The wavenumber of the mode versus gap thickness for Ag under the classical local model and the Landau Damping model, showing no significant difference. c. Propagation length versus gap size for Ag under the classical and Landau Damping models, as well as an ideal metal with no intrinsic damping under the Landau damping model. Landau Damping causes a significant decrease in the propagation length of the waveguide, limiting the maximum achievable propagation length albeit less than when

the wavelength is 850nm. (d) The mode length of the waveguide, showing no change between the Landau Damping and classical models. This indicates that Landau Damping does not limit the achievable confinement in the waveguide.

Appendix C

TUNNELING IN MIM WAVEGUIDES

In Chapter 3, it was found that the onset of Landau Damping did not affect the mode length at all, thus not having any effect on the coupling. This ensures that tunneling (see Introduction), is the limit for confinement in MIM waveguides.

To quantify this limit, the Quantum Corrected Model (QCM) was implemented [39]. This model takes into the account the effects of quantum tunneling through describing the inner dielectric material with the Drude model with plasma frequency equal to that of the metal and a gap dependent damping rate given by:

$$\gamma = \gamma_M e^{2qt} \qquad (C-1)$$

where γ_M is the damping rate of the metal, t is the thickness of the gap, and q is a fitting parameter where in this work $q = 1.12 \cdot 10^{10}/m$.

The parameters of the waveguide were simulated (Fig SC1). No significant change is seen in the wavenumber between the two models until the gap is equal to 0.5nm (Fig SC1a). The propagation length also shows no significant change until a gap of 0.5nm (Fig SC1b). At that point, there is a significant drop in the propagation length which due to the exponential dependence of the damping causes the propagation length to quickly drop down to 1nm. Thus, it is clear that at 0.5nm, the onset of tunneling causes the creation of a significant alternate loss pathway that decreases the propagation to the point the waveguide is no longer useful. We conclude that tunneling is the absolute limit on the confinement in MIM waveguides, and it limits the minimum gap size to ~0.5nm.

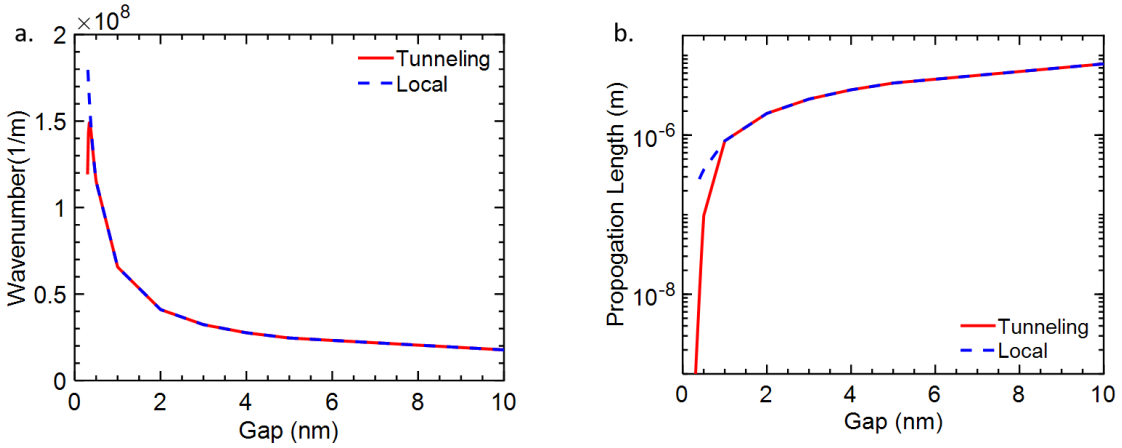

Figure SC1. Effects of tunneling on MIM waveguides. a. The wavenumber of the mode under the classical and QCM (tunneling) models. No significant change is seen until a gap of 0.5nm. b. The propagation length versus gap under the two models. At 0.5nm, tunneling causes the propagation length to significantly decrease, ruining the propagation of the mode and eliminating the operation of the waveguide. Thus a minimum gap of 0.5nm due to tunneling is found.

Appendix D

SIMULATION OF MIM-AIR REFLECTIVITY

In order to calculate the quality factor (Q) of the MIM cavities formed through truncation of an MIM waveguide using the Fabry Perot model, the reflectivity at the MIM-air interface must be known (see eq 4-2). At higher confinements, there is a larger reflectivity at the interface leading to more energy stored in the MIM structure and therefore a higher quality factor. Thus, to accurately calculate the quality factors, it is necessary to calculate the reflectivity (*R)*.

It is difficult to calculate *R* analytically, so instead an FDTD simulation was used. The gap was varied while the inner dielectric value was set to 8 and *R* was simulated (Fig SD1a). It is seen that although *R* is always close to 1, it gets larger and closer to 1 as the gap is decreased. This is due to the increased confinement leading to a larger mode mismatch with air, and thus an increased reflectivity. The inner dielectric was also swept while the gap was fixed to 1nm, showing a smaller *R* at lower dielectric for the same reason (Fig SD1b). These values were integrated into eq 4-2 to compute the Qs seen in chapter 4.

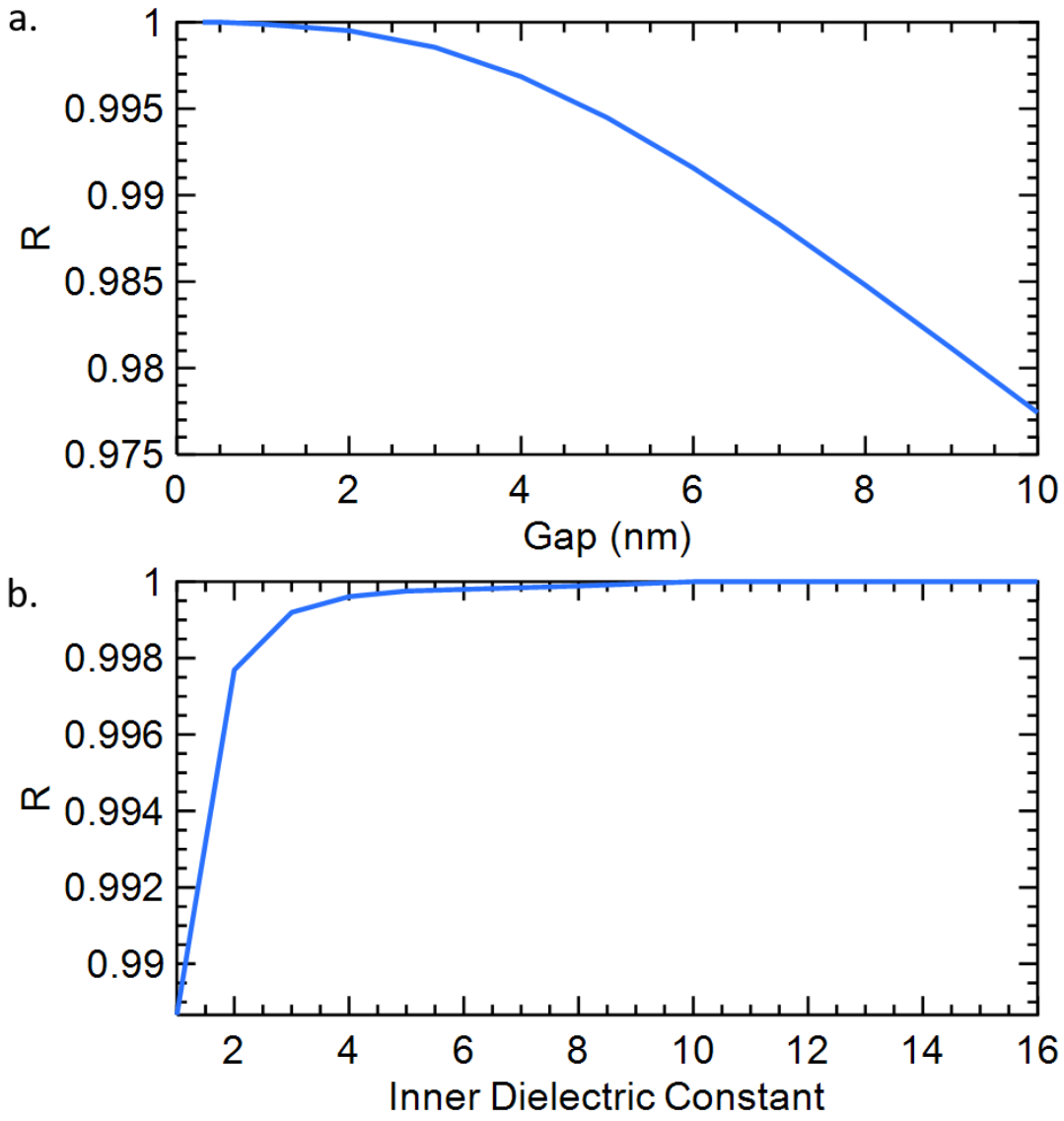

Figure SD1. Reflectivity of air-MIM interface. a. The reflectivity of the interface with a fixed inner dielectric constant of 8 and a varying gap size, showing an increase at smaller gap sizes. b. The reflectivity versus the inner dielectric constant with the gap fixed at 1nm, showing an increase as the dielectric constant increases.